

Published in ApJS, 150, 239 [2004]. This version incorporates corrections due to accepted Erratum ApJS, 153 [2004]

The AST/RO Survey of the Galactic Center Region. I. The Inner 3 Degrees

Christopher L. Martin¹, Wilfred M. Walsh¹, Kecheng Xiao¹, Adair P. Lane¹,
Christopher K. Walker², and Antony A. Stark¹

¹ *Harvard-Smithsonian Center for Astrophysics, 60 Garden St., MS-12, Cambridge, MA 02138*

² *Steward Observatory, University of Arizona, 933 N. Cherry Ave., Tucson, AZ 85721*

cmartin, wwalsh, kxiao, adair, aas@cfa.harvard.edu, cwalker@as.arizona.edu

ABSTRACT

We present fully-sampled maps of 461 GHz CO $J = 4 \rightarrow 3$, 807 GHz CO $J = 7 \rightarrow 6$, and 492 GHz [C I] $^3P_1 \rightarrow ^3P_0$ emission from the inner 3 degrees of the Galactic Center region taken with the Antarctic Submillimeter Telescope and Remote Observatory (AST/RO) in 2001–2002. The data cover $-1.3^\circ < \ell < 2^\circ$, $-0.3^\circ < b < 0.2^\circ$ with 0.5' spacing, resulting in spectra in 3 transitions at over 24,000 positions on the sky. The CO $J = 4 \rightarrow 3$ emission is found to be essentially coextensive with lower- J transitions of CO. The CO $J = 7 \rightarrow 6$ emission is spatially confined to a far smaller region than the lower- J CO lines. The [C I] $^3P_1 \rightarrow ^3P_0$ emission has a spatial extent similar to the low- J CO emission, but is more diffuse. Bright CO $J = 7 \rightarrow 6$ emission is detected in the well-known Galactic Center clouds Sgr A and Sgr B. We also detect CO $J = 4 \rightarrow 3$ and CO $J = 7 \rightarrow 6$ absorption from spiral arms in the galactic disk at velocities near 0 km s⁻¹ along the line of sight to the Galactic Center. Analyzing our CO $J = 7 \rightarrow 6$ and CO $J = 4 \rightarrow 3$ data in conjunction with $J = 1 \rightarrow 0$ ¹²CO and ¹³CO data previously observed with the Bell Laboratories 7-m antenna, we apply a Large Velocity Gradient (LVG) model to estimate the kinetic temperature and density of molecular gas in the inner 200 pc of the Galactic Center region. We show maps of the derived distribution of gas density and kinetic temperature as a function of position and velocity for the entire region. Kinetic temperature was found to decrease from relatively high values (>70 K) at cloud edges to low values (<50 K) in the interiors. Typical gas pressures in the Galactic Center gas are $n(\text{H}_2) \cdot T_{\text{kin}} \sim 10^{5.2} \text{ K cm}^{-3}$. We present an (ℓ, b) map of molecular hydrogen column density derived from our LVG results.

Subject headings: Galaxy:center — Galaxy:kinematics and dynamics — ISM:atoms — ISM:general — ISM:molecules

1. Introduction

Much has been learned about dense gas in the Galactic Center region through radio spectroscopy. Early observations of $F(2 \rightarrow 2)$ OH absorption (Robinson et al. 1964; Goldstein et al. 1964) suggested the existence of copious molecular material within 500 pc of the Galactic Center. This was confirmed by detection of extensive $J = 1 \rightarrow 0$ ^{12}CO emission (Bania 1977; Liszt & Burton 1978). Subsequent CO surveys (Bitran 1987; Stark et al. 1988; Oka et al. 1998; Bitran et al. 1997) have measured this emission with improving coverage and resolution—these surveys show a complex distribution of emission, which is chaotic, asymmetric, and non-planar; there are hundreds of clouds, shells, arcs, rings, and filaments. On scales of 100 pc to 4 kpc, however, the gas is loosely organized around closed orbits in the rotating potential of the underlying stellar bar (Binney et al. 1991). Some CO-emitting gas is bound into clouds and cloud complexes, and some is sheared by tidal forces into a molecular inter-cloud medium of a kind not seen elsewhere in the Galaxy (Stark et al. 1989). This diffuse inter-cloud medium appears in absorption in $F(2 \rightarrow 2)$ OH (McGee 1970; Robinson & McGee 1970), in $(1_{10} \rightarrow 1_{11})$ H_2CO (Scoville, Solomon, & Thaddeus 1972), and in $J = 0 \rightarrow 1$ HCO^+ and HCN (Linke, Stark & Frerking 1981). In contrast, the clouds and cloud complexes are dense, as they must be to survive in the galactic tide, and they appear in spectral lines which are tracers of high density ($n(\text{H}_2) > 10^4 \text{ cm}^{-3}$), such as NH_3 (1, 1) (Güsten, Walmsley, & Pauls 1981) and CS $J = 2 \rightarrow 1$ (Bally et al. 1988). The large cloud complexes, Sgr A, Sgr B, and Sgr C, are among the largest molecular cloud complexes in the Galaxy ($M \gtrsim 10^{6.5} M_\odot$). Such massive clouds must be sinking toward the center of the galactic gravitational well as a result of dynamical friction and hydrodynamic effects (Stark et al. 1991). The deposition of these massive lumps of gas upon the center could fuel a starburst or an eruption of the central black hole (Genzel & Townes 1987).

As prelude to further study of the Galactic Center molecular gas, we would like to determine its physical state—its temperature and density. This involves understanding radiative transfer in CO, the primary tracer of molecular gas. Also useful is an understanding of the atomic carbon lines, [C I], since those lines trace the more diffuse molecular regions, where CO is destroyed by UV radiation but H_2 is still present.

The $J = 1 \rightarrow 0$ ^{12}CO line is often optically thick. Its optical depth can be estimated by studying its isotopomers, ^{13}CO and C^{18}O . In the Galactic Center region, ^{13}CO is $\sim 24\times$ less abundant than ^{12}CO (Penzias 1980; Wilson & Matteucci 1992), and C^{18}O is $\sim 250\times$ less abundant than ^{12}CO (Penzias 1981). Since the radiative and collisional constants of all the isotopomers are similar, the ratio of optical depths in their various spectral lines should simply reflect their relative abundances. Where the lines are optically thin, the line brightnesses should be in the same ratio as the isotopic abundances; where the lines are thick, deviations from the abundance ratios are a measure of optical depth. Bally et al. (1987, 1988) and Stark et al. (1988) produced fully-sampled surveys of ^{12}CO and ^{13}CO in the Galactic Center region. They find that the ratio of the ^{12}CO $J = 1 \rightarrow 0$ to ^{13}CO $J = 1 \rightarrow 0$ line brightness temperatures ($T_{1\rightarrow 0}^{12}/T_{1\rightarrow 0}^{13}$) is typically 10 ± 2 in Galactic Center gas that is far from dense cloud cores. This indicates much of the Galactic

Center ^{12}CO emission is only moderately thick ($\tau_{1\rightarrow 0}^{12} \sim 2$), especially in comparison to the galactic disk outside 3 kpc radius, where $T_{1\rightarrow 0}^{12}/T_{1\rightarrow 0}^{13} \sim 6$ (Polk et al. 1988) is smaller, even though the isotope ratio $^{12}\text{C}/^{13}\text{C} \sim 40$ (Penzias 1980) is larger. Heiligman (1982) and Dahmen et al. (1998) made surveys in C^{18}O $J = 1 \rightarrow 0$. These show ^{12}CO $J = 1 \rightarrow 0$ to C^{18}O $J = 1 \rightarrow 0$ line brightness temperature ratios ($T_{1\rightarrow 0}^{12}/T_{1\rightarrow 0}^{18}$) which vary from 40 to over 200, with typical values near 70, indicating values of $\tau_{1\rightarrow 0}^{12}$ which vary from 3 to less than 1, while the core region of Sgr B2 shows $\tau_{1\rightarrow 0}^{12} \sim 10$.

Determining the excitation temperature of CO works best if emission lines from several J levels have been measured. Lacking such observations, what is often done is to use the brightness temperature of the ^{12}CO $J = 1 \rightarrow 0$ line as a lower limit to the excitation temperature of the $J = 1$ state, $T_{\text{ex}, J=1}$. This estimate can be misleading, because the emission may not fill the telescope beam, diluting the brightness temperature and causing it to be many times smaller than $T_{\text{ex}, J=1}$; as will be apparent from the data to be presented here, this is the usual case for gas in the Galactic Center region.

Moving up the energy ladder, Sawada et al. (2001) surveyed the Galactic Center region in ^{12}CO $J = 2 \rightarrow 1$. They compare their data to the $J = 1 \rightarrow 0$ data of Bitran et al. (1997) and find $T_{2\rightarrow 1}^{12}/T_{1\rightarrow 0}^{12} = 0.96 \pm 0.01$, with little spatial variation. What this means is that almost all the CO in the Galactic Center region has low- J states which are close to local thermodynamic equilibrium (LTE), so that the excitation temperatures $T_{\text{ex}, J}$ of those states are all close to the kinetic temperature, T_{kin} , and the ratio of line brightnesses for transitions between those states are near unity and therefore independent of T_{kin} (cf. Goldreich & Kwan 1974). LTE in the low- J states of CO does not occur under all circumstances in the interstellar medium, but it is very common and appears to be the rule for Galactic Center gas. For each value of T_{kin} and $n(\text{H}_2)$, there will, however, be some value of J above which all higher- J states fail to be populated, because their Einstein A coefficients (which increase as J^3) are so large that the collision rate at that value of T_{kin} and $n(\text{H}_2)$ cannot maintain those states in LTE, and they must therefore be subthermally excited, i.e., $T_{\text{ex}, J} \ll T_{\text{kin}}$. The brightness temperature of the $J \rightarrow J - 1$ line from those states will be significantly less than that of the lower- J states, and the line ratios $T_{J \rightarrow J-1}^{12}/T_{1\rightarrow 0}^{12}$ will be much smaller than unity. Unlike the low- J states, the value of the line ratios from those higher- J states will vary from place to place, depending on T_{kin} , $n(\text{H}_2)$, and radiative transfer effects.

Higher still on the energy ladder, Kim et al. (2002) used the AST/RO telescope to survey a strip at $b = 0^\circ$ in ^{12}CO $J = 4 \rightarrow 3$ and ^{12}CO $J = 7 \rightarrow 6$. They found that even the $T_{4\rightarrow 3}^{12}/T_{1\rightarrow 0}^{12}$ ratio is not far from unity and shows little spatial variation. In contrast, the distribution of $J = 7 \rightarrow 6$ line emission was found to be markedly different from the lower- J transitions. Temperatures and densities could therefore be calculated as a function of position and velocity using the varying value of $T_{7\rightarrow 6}^{12}/T_{4\rightarrow 3}^{12}$ and an estimate of $\tau_{1\rightarrow 0}^{12}$ from the Bally et al. (1987, 1988) and Stark et al. (1988) data. In the current paper, we extend this work to a fully-sampled (ℓ, b) map of the Galactic Center region, and estimate kinetic temperature, T_{kin} , and density, $n(\text{H}_2)$, throughout our mapped area.

Ojha et al. (2001) used AST/RO to make a coarse survey of the Galactic Center region in the ($^3\text{P}_1 \rightarrow ^3\text{P}_0$) line of [C I] at 492 GHz. They find that [C I] is distributed approximately like CO, but that the ratio $T_{\text{C I}}/T_{1 \rightarrow 0}^{12}$ is smaller in the Galactic Center region than in the disk outside 3 kpc. This is attributable to the smaller average optical depth of the $^{12}\text{CO } J = 1 \rightarrow 0$ in this region. The absence of strong spatial variations of $T_{\text{C I}}/T_{1 \rightarrow 0}^{12}$ across their map indicates that the amounts of CO-emitting and [C I]-emitting gas are approximately proportionate across the map. In the current paper we extend this work to a more detailed, fully-sampled (ℓ, b) map in [C I].

In §2, we describe the observatory and the observations. In §3, the full data set in each of the three observed transitions is presented in the form of spatial–spatial maps integrated over the full velocity range, velocity-channel maps, and spatial–velocity maps at several galactic latitudes. In §4, we present a Large Velocity Gradient (LVG) model of the radiative transfer in CO, which allows a determination of kinetic temperature, T_{kin} , and density, $n(\text{H}_2)$. In §5, we present our conclusions.

2. Observations

The observations were performed during the austral winter seasons of 2001 and 2002 at the Antarctic Submillimeter Telescope and Remote Observatory (AST/RO) located at 2847 m altitude at the Amundsen-Scott South Pole Station. This site has very low water vapor, high atmospheric stability and a thin troposphere making it exceptionally good for submillimeter observations (Chamberlin, Lane, & Stark 1997; Lane 1998). AST/RO is a 1.7 m diameter, offset Gregorian telescope capable of observing at wavelengths between 200 μm and 1.3 mm (Stark et al. 1997, 2001). A dual-channel SIS waveguide receiver (Walker et al. 1992; Honingh et al. 1997) was used for simultaneous 461–492 GHz and 807 GHz observations, with double-sideband noise temperatures of 320–390 K and 1050–1190 K, respectively. Telescope efficiency, η_ℓ , estimated using moon scans, skydips, and measurements of the beam edge taper, was 81% at 461–492 GHz and 71% at 807 GHz. Atmosphere-corrected system temperatures ranged from 700 to 4000 K at 461–492 GHz and 9000 to 75,000 K at 807 GHz.

A multiple position-switching mode was used, with emission-free reference positions chosen at least 60' from regions of interest. These reference positions were then shared by a strip of points at constant galactic latitude which were observed five at a time. This mapping mode caused each point in the map to be observed for 60 s per pass through the map. In an attempt to obtain uniform noise over the entire region of interest, subregions were reimaged as often as required.

Emission from the CO $J = 4 \rightarrow 3$ and CO $J = 7 \rightarrow 6$ lines at 461.041 GHz and 806.652 GHz, together with the [C I] $^3\text{P}_1 \rightarrow ^3\text{P}_0$ and [C I] $^3\text{P}_2 \rightarrow ^3\text{P}_1$ lines at 492.262 GHz and 809.342 GHz, was imaged over the Galactic Center region $-1.3^\circ < \ell < 2^\circ$, $-0.3^\circ < b < 0.2^\circ$ with 0.5' spacing in ℓ and b ; i.e., a spacing of a half-beamwidth or less. Smaller selected areas were also observed with longer integration times in the [C I] $^3\text{P}_1 \rightarrow ^3\text{P}_0$ line. Maximum pointing errors were no larger than 1', and

the beam sizes (FWHM) were 103–109'' at 461–492 GHz and 58'' at 807 GHz (Stark et al. 2001). To facilitate comparison of the various transitions, the data were regridded onto a 0.25' grid and smoothed to a FWHM spatial resolution of 2' with a Gaussian filter function.

Two acousto-optical spectrometers (AOSs; Schieder, Tolls, & Winnewisser 1989) were used as backends. The AOSs had 1.07 MHz resolution and 0.75 GHz effective bandwidth, resulting in velocity resolution of 0.65 km s⁻¹ at 461 GHz and 0.37 km s⁻¹ at 807 GHz. To facilitate comparison, the data were then smoothed to a uniform velocity resolution of 1 km s⁻¹. The high frequency observations were made with the CO $J = 7 \rightarrow 6$ line in the lower sideband (LSB). Since the intermediate frequency of the AST/RO system is 1.5 GHz, the [C I] $^3P_2 \rightarrow ^3P_1$ line appears in the upper sideband (USB) and is superposed on the observed LSB spectrum. The local oscillator frequency was chosen so that the nominal line centers appear separated by 100 km s⁻¹ in the double-sideband spectra. The standard chopper wheel calibration technique was employed, implemented at AST/RO by way of regular (every few minutes) observations of the sky and two blackbody loads of known temperature (Stark et al. 2001). Atmospheric transmission was monitored by regular skydips, and known, bright sources were observed every few hours to further check calibration and pointing. At periodic intervals and after tuning, the receivers were manually calibrated against a liquid-nitrogen-temperature load and the two blackbody loads at ambient temperature and about 100 K. The latter process also corrects for the dark current of the AOS optical CCDs. The intensity calibration errors became as large as $\pm 15\%$ during poor weather periods.

Once taken, the data in this survey were reduced using the COMB data reduction package. After elimination of scans deemed faulty for various instrumental or weather-related reasons ($\lesssim 2\%$ of the total dataset), linear baselines were removed from the spectra in all species by excluding regions where the CO $J = 1 \rightarrow 0$ spectra showed emission greater than $T_A^* \geq 1$ K. This allowed known emission in the Galactic Center region to be readily excluded from the baseline fitting procedure and was generally sufficient. In a few cases, usually due to higher than average T_{rms} for a given reduced spectrum, this method fails and artifacts (e.g., vertical lines in the longitude–velocity maps) appear.

While the original intent was to make T_{rms} as uniform as possible across the entire map, this was not always possible. For the CO $J = 4 \rightarrow 3$ transition, T_{rms} in 1 km s⁻¹ wide channels with 2' spatial smoothing is on average $\lesssim 0.3$ K except in the region $1.8^\circ > \ell > 1.5^\circ$ where $T_{\text{rms}} \lesssim 0.8$ K. The [C I] $^3P_1 \rightarrow ^3P_0$ transition has $T_{\text{rms}} \lesssim 0.5$ K in 1 km s⁻¹ channels for the central region of $1.0^\circ > \ell > -0.5^\circ$, $T_{\text{rms}} \lesssim 1.0$ K for $\ell > 1.0^\circ$, and $T_{\text{rms}} \lesssim 2$ K for $\ell < -0.5^\circ$. Finally, for CO $J = 7 \rightarrow 6$ (ignoring the occasional baseline feature), $T_{\text{rms}} \lesssim 0.8$ K in 1 km s⁻¹ channels for $\ell > 0.7$ and $-0.5^\circ > \ell > -0.8^\circ$, and $T_{\text{rms}} \lesssim 2$ K elsewhere.

3. Data Presentation

Sample spectra at the respective positions of peak CO $J = 7 \rightarrow 6$ emission toward the Sgr A ($\ell = 0^\circ.00$, $b = -0^\circ.07$), Sgr B ($\ell = 0^\circ.66$, $b = -0^\circ.05$), Sgr C ($\ell = -0^\circ.45$, $b = -0^\circ.20$) (CO $J = 4 \rightarrow 3$ emission peak), and $\ell \simeq 1^\circ.3$ ($\ell = 1^\circ.25$, $b = -0^\circ.05$) molecular complexes are shown in Fig. 1. The CO $J = 4 \rightarrow 3$, CO $J = 7 \rightarrow 6$, and [C I] $^3P_1 \rightarrow ^3P_0$ data are from the AST/RO survey, while the CO $J = 1 \rightarrow 0$, $^{13}\text{CO } J = 1 \rightarrow 0$, and CS $J = 2 \rightarrow 1$ data are from the Bell Laboratories (BL) 7-m telescope (Stark et al. 1988; Bally et al. 1987, 1988). All of the spectra are from datacubes smoothed to $2'$ resolution.

The CO $J = 4 \rightarrow 3$ profile toward Sgr B resembles the CO $J = 1 \rightarrow 0$ profile, with similar linewidth and a prominent self-absorption feature at $v_{\text{LSR}} = 60 \text{ km s}^{-1}$. The total velocity extent is somewhat smaller in CO $J = 4 \rightarrow 3$ on the negative velocity side. In contrast, the [C I] $^3P_1 \rightarrow ^3P_0$ and CO $J = 7 \rightarrow 6$ lines, as well as the ^{13}CO , show peak emission at the self-absorption velocity, suggesting these lines are less optically thick. It is important to note that the strong feature at negative velocities in the CO $J = 7 \rightarrow 6$ spectrum toward Sgr B is due to superposed emission in the 809 GHz ($^3P_2 \rightarrow ^3P_1$) line of [C I] in the image sideband.

Fig. 2 presents spatial–spatial (ℓ, b) maps integrated over velocity for the three transitions observed with AST/RO¹ and, for comparison, the three transitions observed at the BL 7-m. All six maps have been smoothed to the same $2'$ spatial resolution. The regions with $\ell > 0^\circ.9$ and $\ell < -0^\circ.5$ in the $^{13}\text{CO } J = 1 \rightarrow 0$ map were observed with sparser sampling than the rest of the map (Bally et al. 1987). The most striking result is that CO $J = 4 \rightarrow 3$ emission in the Galactic Center region is essentially coextensive with the emission from the lower J transitions of CO. This contrasts sharply with the outer Galaxy where CO $J = 4 \rightarrow 3$ emission is rather less extensive than CO $J = 1 \rightarrow 0$. In all six maps, the brightest emission occurs primarily at negative latitudes. Four major cloud complexes are seen in the CO $J = 1 \rightarrow 0$, CO $J = 4 \rightarrow 3$, and $^{13}\text{CO } J = 1 \rightarrow 0$ maps, from left to right: the complex at $\ell \simeq 1^\circ.3$, the Sgr B complex near $\ell \simeq 0^\circ.7$, the Sgr A cloud near $\ell \simeq 0^\circ.0$, and the Sgr C cloud near ($\ell \simeq -0^\circ.45$, $b \simeq -0^\circ.2$). As noted by Kim et al. (2002), the CO $J = 7 \rightarrow 6$ emission is much more spatially confined than the lower- J CO transitions. In contrast, the [C I] emission is comparable in spatial extent to the low- J CO emission, but its distribution appears somewhat more diffuse (less peaked). The Sgr C cloud is much less prominent in the [C I] map than in the other five transitions. The noise in the [C I] map at $\ell < -0^\circ.7$ is greater than that in the rest of the map due to shorter integration times.

Figs. 3–5 present spatial–spatial maps in successive 10 km s^{-1} wide velocity ranges in the CO $J = 4 \rightarrow 3$, [C I] $^3P_1 \rightarrow ^3P_0$, and CO $J = 7 \rightarrow 6$ lines, respectively. For each spectral line, velocity channels centered at velocities from -165 km s^{-1} to $+185 \text{ km s}^{-1}$ (see upper left corner of

¹Complete FITS datacubes of the three AST/RO datasets are archived with the electronic edition of this paper. As new data becomes available updated versions will be posted at http://cfa-www.harvard.edu/~adair/AST_RO/abc.html.

each map) are displayed. In each map, the integrated intensity has been divided by 10 km s^{-1} so that the intensity color scale is a reasonably good indicator of corrected average antenna temperature, $\langle T_A^* \rangle$.

Spatial–velocity maps at 12 different values of galactic latitude are shown in Figs. 6–8 for CO $J = 4 \rightarrow 3$, [C I] $^3\text{P}_1 \rightarrow ^3\text{P}_0$, and CO $J = 7 \rightarrow 6$, respectively. All major structures in the galactic core can be identified in these maps, including Sgr A, Sgr B, Sgr C, and the $\ell \simeq 1.3$ complex. The 300 pc molecular ring shows up prominently in both the [C I] and CO $J = 4 \rightarrow 3$ (ℓ – v) maps, running in a straight, continuous line from ($\ell \sim 2^\circ, v_{\text{LSR}} \sim 220 \text{ km s}^{-1}$) to ($\ell \sim -0.9^\circ, v_{\text{LSR}} \sim 120 \text{ km s}^{-1}$), and from ($\ell \sim 1.5^\circ, v_{\text{LSR}} \sim -20 \text{ km s}^{-1}$) to ($\ell \sim -0.9^\circ, v_{\text{LSR}} \sim -180 \text{ km s}^{-1}$). There is little or no evidence that the CO $J = 7 \rightarrow 6$ line is excited into emission in the 300 pc ring. Also absent in the CO $J = 7 \rightarrow 6$ line is any trace of the 3 kpc arm, which is prominent in CO $J = 1 \rightarrow 0$ emission. The 3 kpc arm must contain little dense, warm gas. Foreground absorption by spiral arms in the galactic disk is seen at velocities near 0 km s^{-1} in CO $J = 4 \rightarrow 3$ and [C I] $^3\text{P}_1 \rightarrow ^3\text{P}_0$. A hint of this absorption feature is seen in CO $J = 7 \rightarrow 6$.

4. LVG Model

The large velocity gradient (LVG) approximation (Goldreich & Kwan 1974) simplifies radiative transfer analysis of molecular lines. Imagine a small volume within a molecular cloud, in which a molecule emits a photon. The volume is sufficiently small that all velocities within it are thermal, and temperature and density are constant. It is surrounded by other small volumes which have similar temperature and density, and whose internal velocities are also thermal, but the velocities of these other volumes are different from that of the volume which emitted the photon because of velocity gradients within the molecular cloud. In LVG, it is assumed that if the photon is going to be absorbed, rather than escaping from the cloud, it can only be absorbed in nearby volumes, those volumes whose velocities are close to the velocity of the emitting volume. In this case ‘close’ means close enough that the thermal linewidths overlap. As the emitted photon travels away from its point of origin, it passes through nearby volumes where it has a chance to be absorbed because the thermal motion of some of the molecules causes them to have the same velocity as the emitting molecule. At some distance from the point of emission, this will no longer be true because of velocity gradients, and in LVG it is assumed that the photon then escapes from the cloud. The velocity gradient is ‘large’ in the sense that the region of possible absorption is small compared to the cloud as a whole, so it can be assumed that in effect the photon was absorbed at its point of origin. This achieves a great simplification in making the radiative transfer problem entirely ‘local’, while allowing for the possibility of absorption. The probability that a photon will escape from the cloud and become observable then depends only on the local physical and chemical properties of the emitting gas and on the value of the velocity gradient. The emitting cloud can then be modeled using only a few parameters, yet the radiative transfer is realistic enough to compare to observations. The parameters of the model can then be adjusted to fit the data, and an estimate

of those parameters is thereby achieved. Ossenkopf (1997) has shown that such estimates are robust, in the sense that the parameter values derived are often approximately correct, even in circumstances where the assumptions of the LVG approximation are violated.

We will use this LVG methodology to estimate the kinetic temperature, T_{kin} , and the number density of molecular hydrogen, $n(\text{H}_2)$, throughout the Galactic Center region. Due to the high velocity dispersions characteristic of the Galactic Center, the LVG approximation is most likely valid over much of the mapped region. The LVG approximation does not apply to some of our data: the foreground absorption by spiral arms is clearly not local to the emitting gas in the Sgr A cloud. It should be kept in mind that the LVG approximation is an *Ansatz* which allows us to estimate the physical properties of the Galactic Center gas in what otherwise would be an untenably complex modeling problem.

Our cloud model was developed by M. Yan and S. Kim. It has plane-parallel cloud geometry. It uses CO collisional rates determined by Turner (1995) and uses newly-derived values for the H_2 ortho-to-para ratio (≈ 2) (Rodríguez-Fernández et al. 2000) and for the collisional quenching rate of CO by H_2 impact (Balakrishnan, Yan, & Dalgarno 2002). The model has two input parameters: the ratio of ^{12}CO to ^{13}CO abundance, and the ratio $X(\text{CO})/\nabla V$, where $X(\text{CO})$ is the fractional CO abundance parameter and ∇V is the velocity gradient. As discussed in §1, the abundance ratio $^{12}\text{CO}/^{13}\text{CO}$ is 24 in the Galactic Center region (Penzias 1980; Langer & Penzias 1990; Wilson & Mattheucci 1992; Langer & Penzias 1993). We will use a value $X(\text{CO})/\nabla V = 10^{-4.5} \text{ pc km}^{-1} \text{ s}$, assuming that the $^{12}\text{CO}/\text{H}_2$ ratio is 10^{-4} and the velocity gradient within the Galactic Center gas is a uniform $3 \text{ km s}^{-1} \text{ pc}^{-1}$. Dahmen et al. (1998) estimated that ∇V is $3 \text{ km s}^{-1} \text{ pc}^{-1}$ to $6 \text{ km s}^{-1} \text{ pc}^{-1}$, and indeed these are typical slopes of position-velocity features in Galactic Center maps. There is, however, no reason to suppose that a single value of ∇V applies throughout the Galactic Center region, or even that ∇V is constant within a single cloud. This is a weak point in the analysis, because in the LVG analysis $n(\text{H}_2) \propto (\nabla V)^{0.6}$, when all other parameters are held fixed.

For each observed point, we take the brightness temperature ratios $T_{7 \rightarrow 6}^{12}/T_{4 \rightarrow 3}^{12}$ and $T_{1 \rightarrow 0}^{13}/T_{1 \rightarrow 0}^{12}$, using the same methodology as Kim et al. (2002), to determine T_{kin} and $n(\text{H}_2)$. Fig. 9 is a smoothed representation of the relationships generated by our LVG model. Note that our model, using the $T_{7 \rightarrow 6}^{12}/T_{4 \rightarrow 3}^{12}$ ratio, is particularly sensitive to variations in density and temperature near $T_{\text{kin}} \sim 40\text{K}$ and $n(\text{H}_2) \sim 10^4 \text{ cm}^{-3}$, and that its range of validity extends a factor of ~ 20 in density and ~ 4 in temperature around these values. Much of the Galactic Center gas falls within this range; the gas which does not could be studied using various other transitions of the CO isotopomers, or using other species such as [C I] and CS.

Fig. 10 shows the output of our LVG analysis for T_{kin} as spatial-velocity maps for 6 different values of galactic latitude, while Fig. 11 does the same for $n(\text{H}_2)$. White regions on the maps indicate areas where either the LVG inversion did not converge or where there is missing data from the maps of the four transitions used. The LVG model strains to fit in regions where $T_{1 \rightarrow 0}^{13}/T_{1 \rightarrow 0}^{12}$ is

so small it approaches the value of the isotope ratio (1/24). Where $T_{1\rightarrow 0}^{13}/T_{1\rightarrow 0}^{12} < 0.1$, that is, where the $J = 1 \rightarrow 0$ CO line is less optically thick, the model assigns high kinetic temperatures (cf. the bottom of Fig. 9). T_{kin} starts high in the lower density regions. This is physically reasonable since the edges of these complexes are likely to be of lower density and externally heated. Moving into the interior of the complexes, we find a surprisingly uniform temperature of $T_{\text{kin}} \sim 50$ K and density of $n(\text{H}_2) \sim 10^{3.5} \text{ cm}^{-3}$. This indicates a typical pressure $n(\text{H}_2) \cdot T_{\text{kin}} \sim 10^{5.2} \text{ K cm}^{-3}$. Exceptional are the density peak at Sgr B and the foreground material along $v_{\text{LSR}} \simeq 0 \text{ km s}^{-1}$. The breakdown of LVG assumptions in the foreground absorbing material renders the T_{kin} and $n(\text{H}_2)$ results suspect if not outright invalid near the absorbing material.

Fig. 12 shows the estimated column density as determined by integrating the LVG spatial density and dividing by ∇V . The region $-60 < v_{\text{LSR}} < 20 \text{ km s}^{-1}$ is excluded in order to avoid contamination by the foreground material for which the LVG analysis is invalid; the actual total column density should therefore be somewhat larger than the value shown here. Also, there are a few places where the LVG model fails to converge even though the lines are strong and the density is presumably high—the density in those spots does not contribute to our estimate of the column density. There is an overall factor of order unity uncertainty in the scaling of this map due to likely errors in our assumed value of ∇V . The map clearly shows the density enhancement toward Sgr A and Sgr B and the relatively high density of the material surrounding and connecting them. In the closed-orbit paradigm of Binney et al. (1991), this material is in x_2 orbits.

5. Conclusions

1. We have mapped the inner 3° of the Galaxy in 461 GHz CO $J = 4 \rightarrow 3$, 807 GHz CO $J = 7 \rightarrow 6$, and 492 GHz [C I] $^3\text{P}_1 \rightarrow ^3\text{P}_0$ emission. Sgr A, Sgr B, Sgr C, and the 300 pc molecular ring are easily identified.
2. The CO $J = 4 \rightarrow 3$ emission is found to be essentially coextensive with lower- J transitions of CO. The CO $J = 7 \rightarrow 6$ emission is spatially confined to a far smaller region than the lower- J CO lines. The [C I] $^3\text{P}_1 \rightarrow ^3\text{P}_0$ emission has a spatial extent similar to the low- J CO emission, but is more diffuse.
3. Consistent with Kim et al. (2002), we find the $T_{4\rightarrow 3}^{12}/T_{1\rightarrow 0}^{12}$ line ratio is approximately constant and not far from unity over much of the mapped region. In contrast, the $T_{7\rightarrow 6}^{12}/T_{4\rightarrow 3}^{12}$ line ratio is found to vary significantly.
4. For each observed point, $T_{7\rightarrow 6}^{12}/T_{4\rightarrow 3}^{12}$ line ratios, together with $T_{1\rightarrow 0}^{13}/T_{1\rightarrow 0}^{12}$ line ratios, were used to estimate kinetic temperatures and molecular hydrogen volume densities. Kinetic temperature was found to decrease from relatively high values (>70 K) at cloud edges to low values (<50 K) in the interiors. Molecular hydrogen densities, $n(\text{H}_2)$, ranged up to the limit of our ability to determine via our LVG analysis, $\sim 10^{4.5} \text{ cm}^{-3}$.

5. Typical gas pressures in the Galactic Center gas are $n(\text{H}_2) \cdot T_{\text{kin}} \sim 10^{5.2} \text{ K cm}^{-3}$, while typical virial pressures are $n(\text{H}_2) \cdot T_{\text{virial}} \sim 10^{6.8} \text{ K cm}^{-3}$. These values can be compared to the typical gas pressures in molecular clouds near the Sun $\sim 10^{3.4} \text{ K cm}^{-3}$, the typical virial pressure in molecular clouds near the Sun $\sim 10^5 \text{ K cm}^{-3}$, and the ambient pressure of the interstellar medium near the Sun $\sim 10^4 \text{ K cm}^{-3}$ (Dickey & Lockman 1990).

We thank the receiver group at the U. of Arizona for their assistance; R. Schieder, J. Stutzki, and colleagues at U. Köln for their AOSs; J. Kooi and R. Chamberlin of Caltech, G. Wright of PacketStorm Communications, and K. Jacobs of U. Köln for their work on the instrumentation; M. Yan and S. Kim for the use of their LVG code; and J. Carlstrom for comments on the manuscript. This research was supported in part by the National Science Foundation under a cooperative agreement with the Center for Astrophysical Research in Antarctica (CARA), grant number NSF OPP 89-20223. CARA is a National Science Foundation Science and Technology Center. Support was also provided by NSF grant number OPP-0126090.

REFERENCES

- Balakrishnan, N., Yan, M., & Dalgarno, A. 2002, *ApJ*, 568, 443
- Bally, J., Stark, A. A., Wilson, R. W., & Henkel, C. 1987, *ApJS*, 65, 13
- . 1988, *ApJ*, 324, 223
- Bania, T. M. 1977, *ApJ*, 216, 381
- Binney, J., Gerhard, O. E., Stark, A. A., Bally, J., & Uchida, K. I. 1991, *MNRAS*, 252, 210
- Bitran, M., Alvarez, H., Bronfman, L., May, J., & Thaddeus, P. 1997, *A&AS*, 125, 99
- Bitran, M. E. 1987, PhD thesis, University of Florida
- Chamberlin, R. A., Lane, A. P., & Stark, A. A. 1997, *ApJ*, 476, 428
- Dahmen, G., Hüttemeister, S., Wilson, T. L., & Mauersberger, R. 1998, *A&A*, 331, 959
- Dickey, J. M. & Lockman, F. J. 1990, *ARA&A*, 28, 215
- Genzel, R. & Townes, C. H. 1987, *ARA&A*, 25, 377
- Goldreich, P. & Kwan, J. 1974, *ApJ*, 189, 441
- Goldstein, S. J., Gundermann, E. J., Penzias, A. A., & Lilley, A. E. 1964, *Nature*, 203, 65
- Güsten, R., Walmsley, C. M., & Pauls, T. 1981, *A&A*, 103, 197

- Heiligman, G. M. 1982, PhD thesis, Princeton University
- Honigh, C. E., Haas, S., Hottgenroth, D., Jacobs, K., & Stutzki, J. 1997, in Eighth International Symposium on Space Terahertz Technology, 92
- Kim, S., Martin, C. L., Stark, A. A., & Lane, A. P. 2002, *ApJ*, 580, 896
- Lane, A. P. 1998, in *Astrophysics From Antarctica*, ed. G. Novack & R. H. Landsberg, Vol. 141 (ASP Conference Series), 289
- Langer, W. D. & Penzias, A. A. 1990, *ApJ*, 357, 477
- . 1993, *ApJ*, 408, 539
- Linke, R. A., Stark, A. A., & Frerking, M. A. 1981, *ApJ*, 243, 147
- Liszt, H. S. & Burton, W. B. 1978, *ApJ*, 226, 790
- McGee, R. X. 1970, *Aust. J. Phys.*, 23, 541
- Ojha, R., Stark, A. A., Hsieh, H. H., Lane, A. P., Chamberlin, R. A., Bania, T. M., Bolatto, A. D., Jackson, J. M., & Wright, G. A. 2001, *ApJ*, 548, 253
- Oka, T., Hasegawa, T., Sato, F., Tsuboi, M., & Miyazaki, A. 1998, *ApJS*, 118, 455
- Ossenkopf, V. 1997, *New Astronomy*, 2, 365
- Penzias, A. A. 1980, *Science*, 208, 663
- . 1981, *ApJ*, 249, 518
- Polk, K. S., Knapp, G. R., Stark, A. A., & Wilson, R. W. 1988, *ApJ*, 332, 432
- Robinson, B. J., Gardner, F. F., vanDamme, K. J., & Bolton, J. G. 1964, *Nature*, 202, 989
- Robinson, B. J. & McGee, R. X. 1970, *Aust. J. Phys.*, 23, 405
- Rodríguez-Fernández, N. J., Martín-Pintado, J., de Vicente, P., Fuente, A., Hüttemeister, S., Wilson, T. L., & Kunze, D. 2000, *A&A*, 356, 695
- Sawada, T., Hasegawa, T., Handa, T., Morino, J., Oka, T., Booth, R., Bronfman, L., Hayashi, M., Luna Castellanos, A., Nyman, L., Sakamoto, S., Seta, M., Shaver, P., Sorai, K., & Usuda, K. S. 2001, *ApJS*, 136, 189
- Schieder, R., Tolls, V., & Winnewisser, G. 1989, *Experimental Astronomy*, 1, 101
- Scoville, N. Z., Solomon, P. M., & Thaddeus, P. 1972, *ApJ*, 172, 335

- Stark, A. A., Bally, J., Balm, S. P., Bania, T. M., Bolatto, A. D., Chamberlin, R. A., Engargiola, G., Huang, M., Ingalls, J. G., Jacobs, K., Jackson, J. M., Kooi, J. W., Lane, A. P., Lo, K.-Y., Marks, R. D., Martin, C. L., Mumma, D., Ojha, R., Schieder, R., Staguhn, J., Stutzki, J., Walker, C. K., Wilson, R. W., Wright, G. A., Zhang, X., Zimmermann, P., & Zimmermann, R. 2001, *PASP*, 113, 567
- Stark, A. A., Bally, J., Gerhard, O. E., & Binney, J. 1991, *MNRAS*, 248, 14P
- Stark, A. A., Bally, J., Knapp, G. R., & Wilson, R. W. 1988, in *Molecular Clouds in the Milky Way and External Galaxies*, ed. R. L. Dickman, R. L. Snell, & J. S. Young (Springer-Verlag), 303
- Stark, A. A., Bally, J., Wilson, R. W., & Pound, M. W. 1989, in *IAU Symp. 136: The Center of the Galaxy*, ed. M. Morris (Kluwer), 129
- Stark, A. A., Chamberlin, R. A., Cheng, J., Ingalls, J., & Wright, G. 1997, *Rev. Sci. Instr.*, 68, 2200
- Turner, B. E. 1995, *ApJ*, 455, 556
- Walker, C. K., Kooi, J. W., Chan, M., Leduc, H. G., Schaffer, P. L., Carlstrom, J. E., & Phillips, T. G. 1992, *Int. J. Infrared Millimeter Waves*, 13, 785
- Wilson, T. L. & Matteucci, F. 1992, *A&A Rev.*, 4, 1

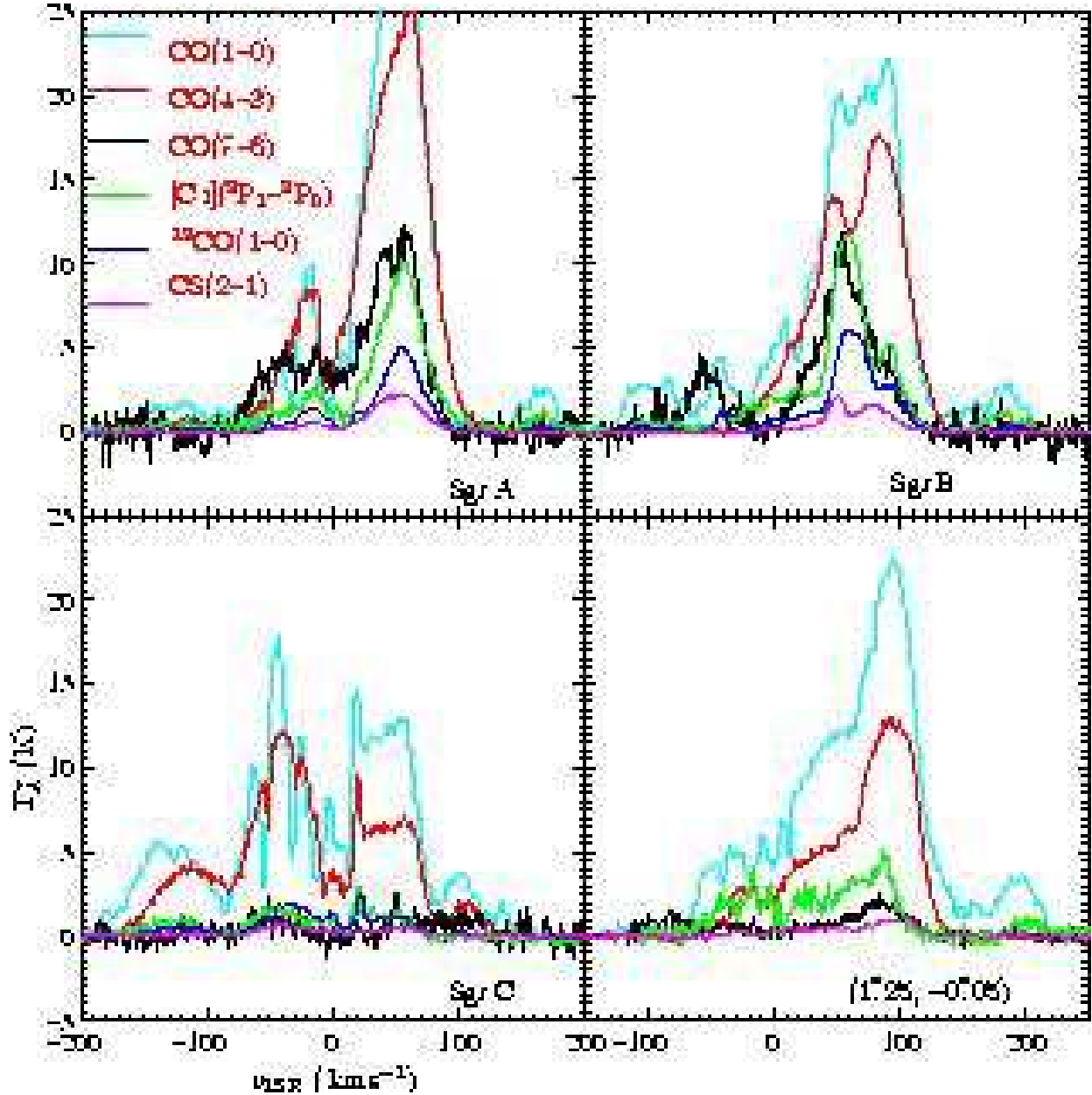


Fig. 1.— Spectra toward the respective positions of peak CO $J = 7 \rightarrow 6$ emission in the Sgr A ($\ell = 0^\circ.00$, $b = -0^\circ.07$), Sgr B ($\ell = 0^\circ.66$, $b = -0^\circ.05$), Sgr C ($\ell = -0^\circ.45$, $b = -0^\circ.20$) (CO $J = 4 \rightarrow 3$ emission peak), and $\ell \simeq 1.3$ ($\ell = 1^\circ.25$, $b = -0^\circ.05$) clouds (as indicated at lower right in each frame) in 6 different transitions, as indicated by the color identifications at upper left. The 461 GHz CO $J = 4 \rightarrow 3$, 807 GHz CO $J = 7 \rightarrow 6$, and 492 GHz [C I] $^3P_1 \rightarrow ^3P_0$ data are from the AST/RO survey (*this paper*), and the 115 GHz CO $J = 1 \rightarrow 0$, 110 GHz $^{13}\text{CO } J = 1 \rightarrow 0$, and 98 GHz CS $J = 2 \rightarrow 1$ data are from the Bell Laboratories 7-m telescope (Stark et al. 1988; Bally et al. 1987, 1988).

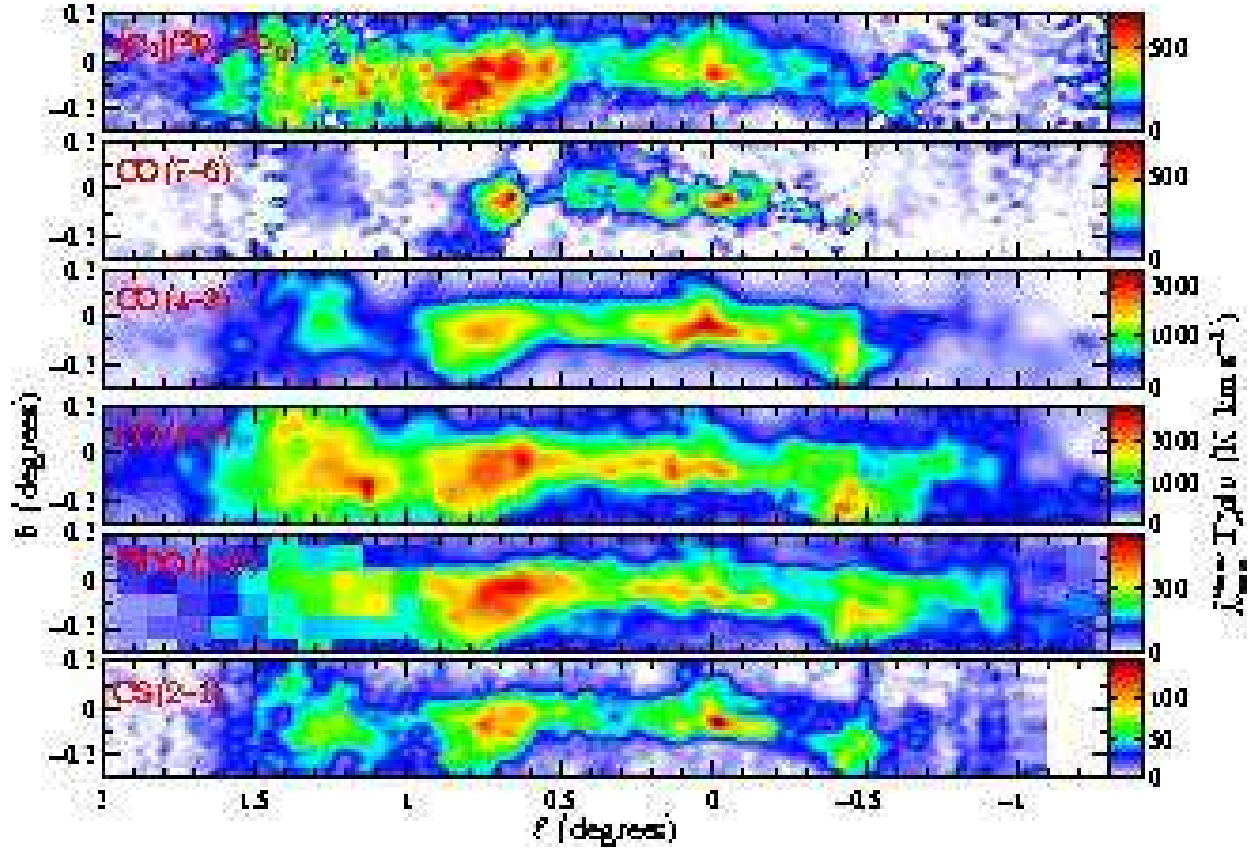


Fig. 2.— Spatial-spatial (ℓ, b) integrated intensity maps for the 3 transitions observed with AST/RO (*top 3 panels*) and, for comparison, the 3 transitions observed at the BL 7-m (Stark et al. 1988; Bally et al. 1987, 1988) (*bottom 3 panels*). Transitions are identified at left on each panel. The emission is integrated over all velocities where data are available. These values of (v_{min}, v_{max}) are: [C I], $(-90, 150)$; CO(7-6), $(-30, 120)$; CO(4-3), $(-150, 150)$; CO(1-0), $(-150, 150)$; $^{13}\text{CO}(1-0)$, $(-150, 150)$; CS(2-1), $(-150, 150)$. All 6 maps have been smoothed to the same $2'$ resolution. This figure has been corrected as noted in the erratum.

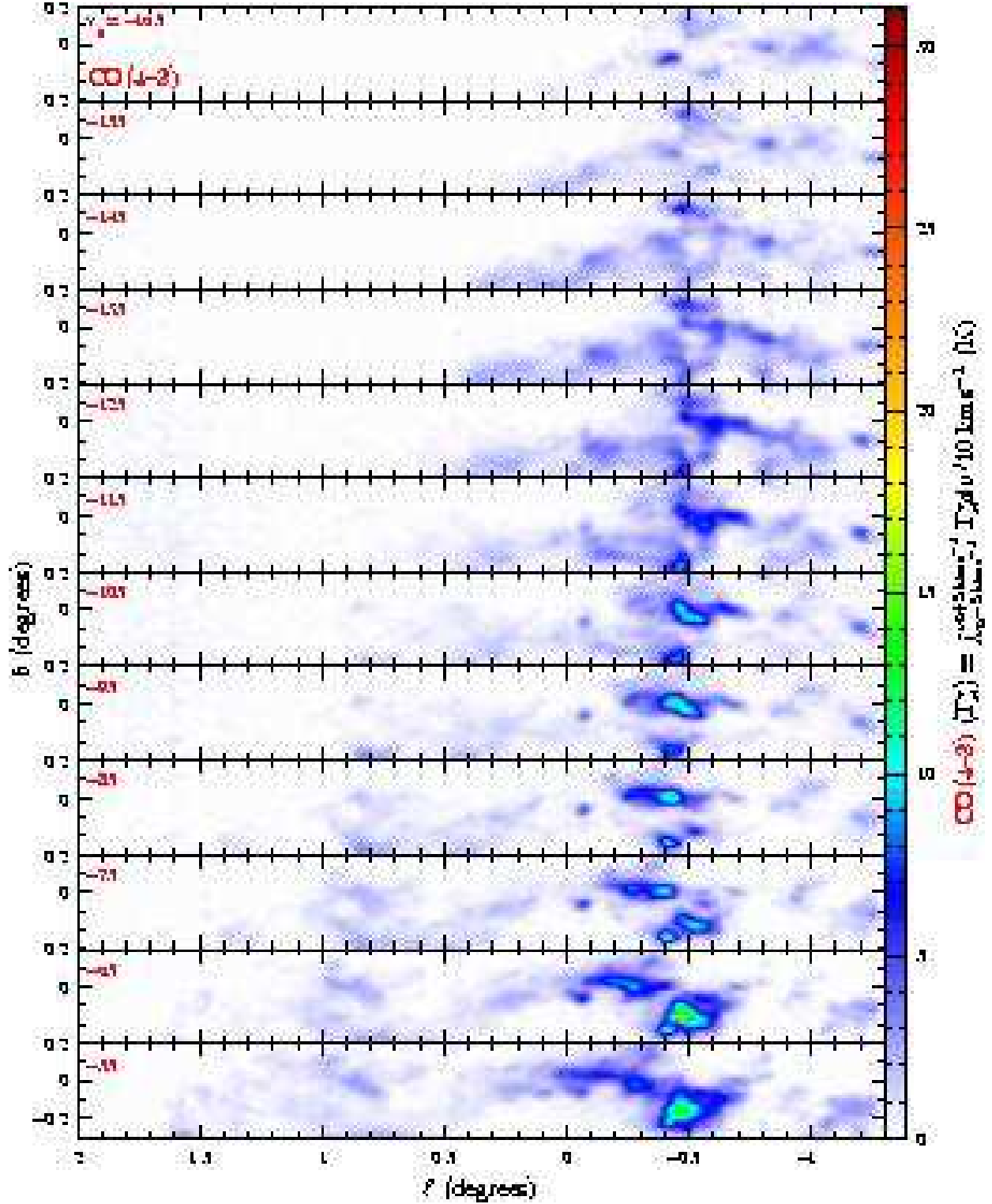


Fig. 3.— False color velocity-channel maps for the CO $J = 4 \rightarrow 3$ transition toward the Galactic Center. Each subpanel shows a 10 km s^{-1} velocity bin, centered at the velocity shown in the upper lefthand corner. The integrated emission in K km s^{-1} has been divided by the 10 km s^{-1} width of the bin so that the color scale at right indicates $\langle T_A^* \rangle$. This figure has been corrected as noted in the erratum.

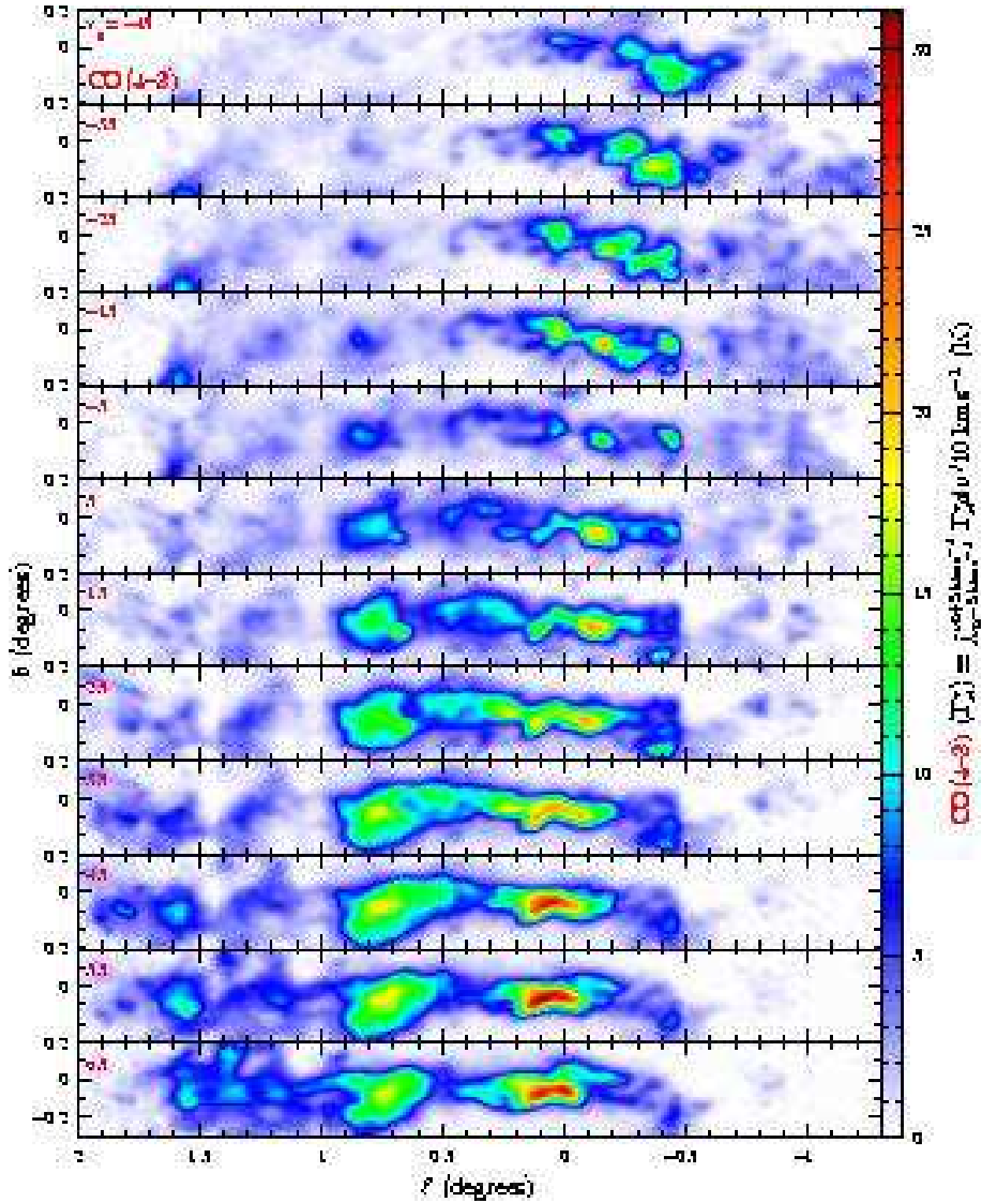


Fig. 3.— *Continued*

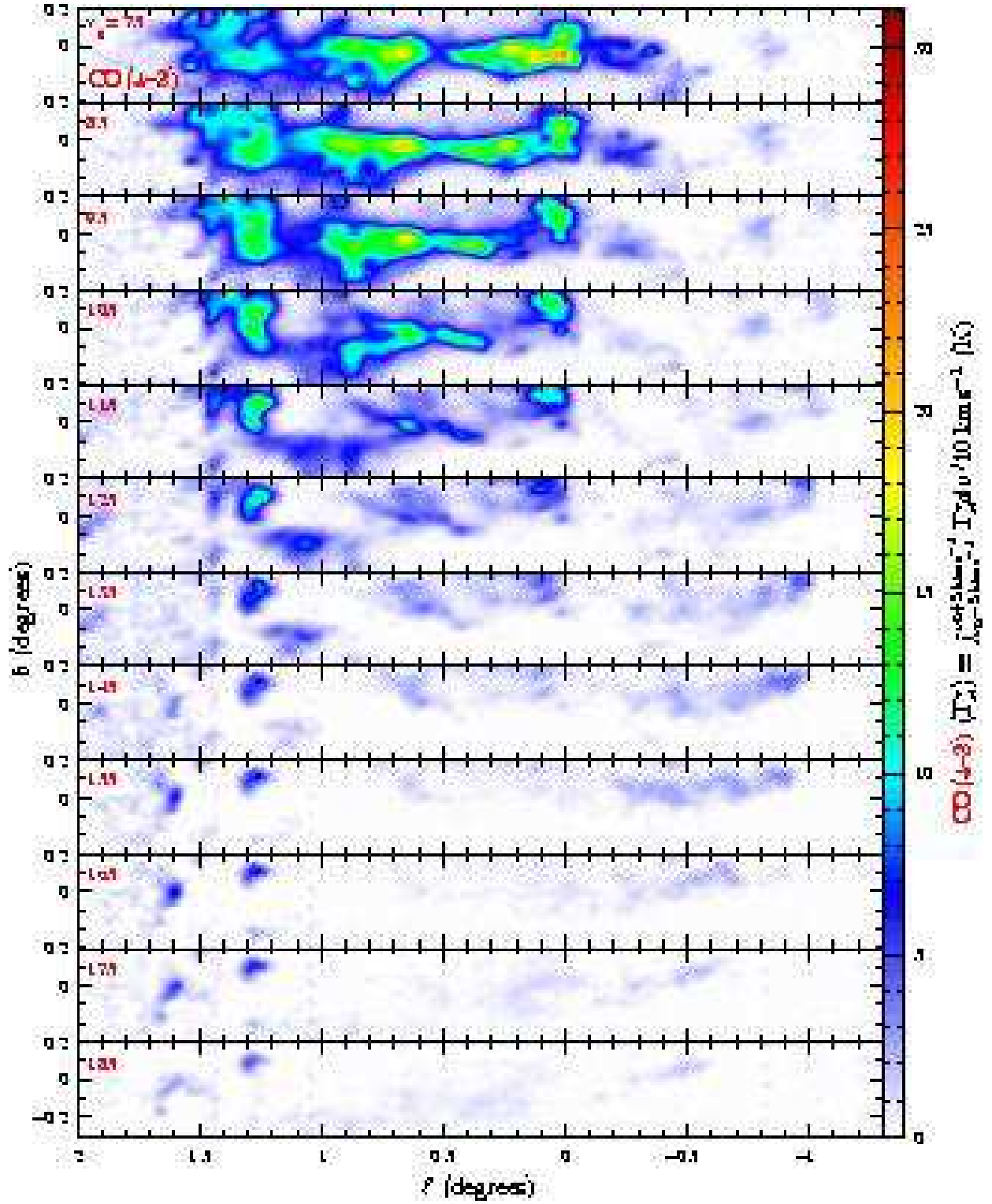


Fig. 3.— *Continued*

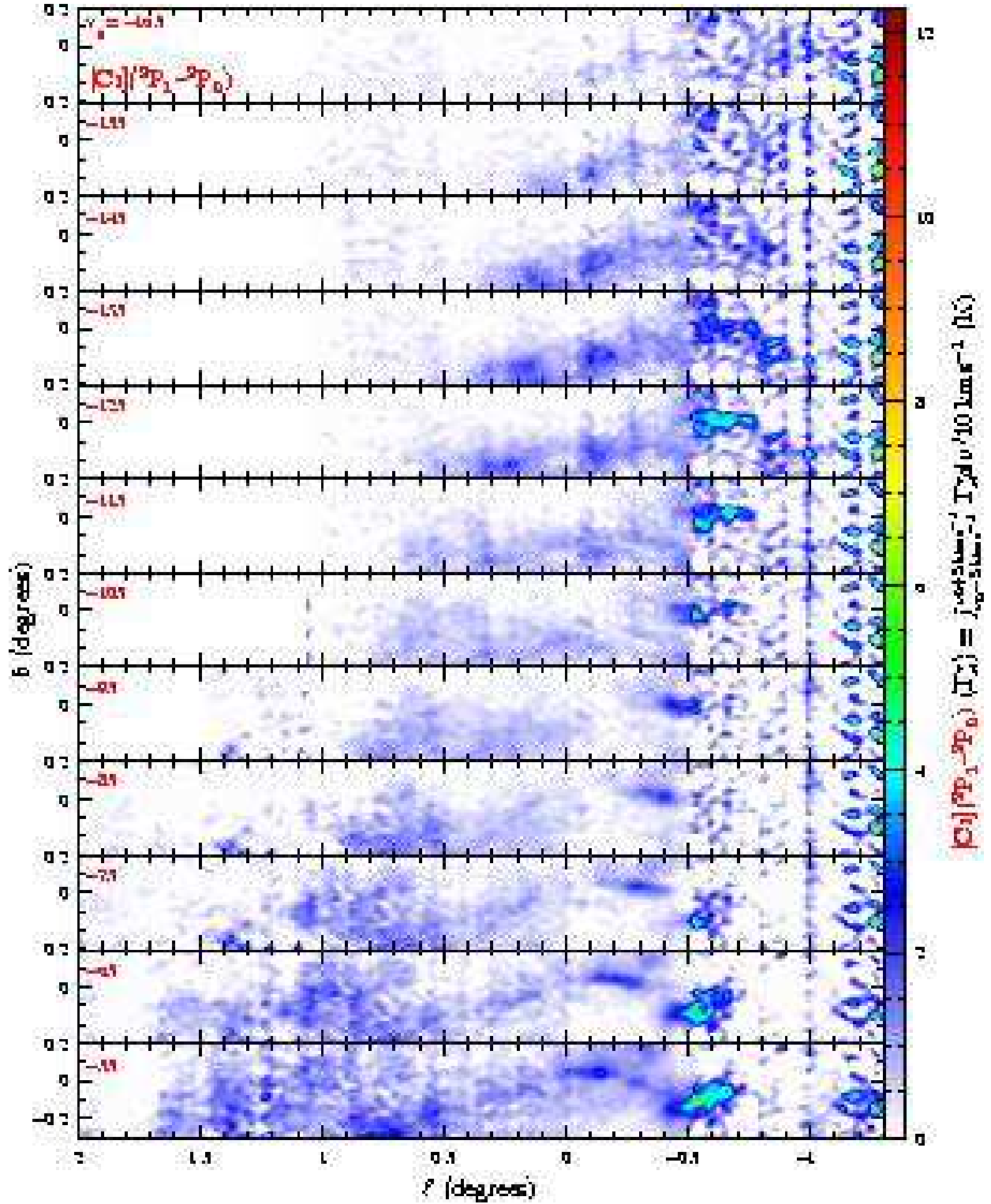


Fig. 4.— False color velocity-channel maps for the [C I] $^3P_1 \rightarrow ^3P_0$ transition toward the Galactic Center. Each subpanel shows a 10 km s^{-1} velocity bin, centered at the velocity shown in the upper lefthand corner. The integrated emission in K km s^{-1} has been divided by the 10 km s^{-1} width of the bin so that the color scale at right indicates $\langle T_A^* \rangle$. This figure has been corrected as noted in the erratum.

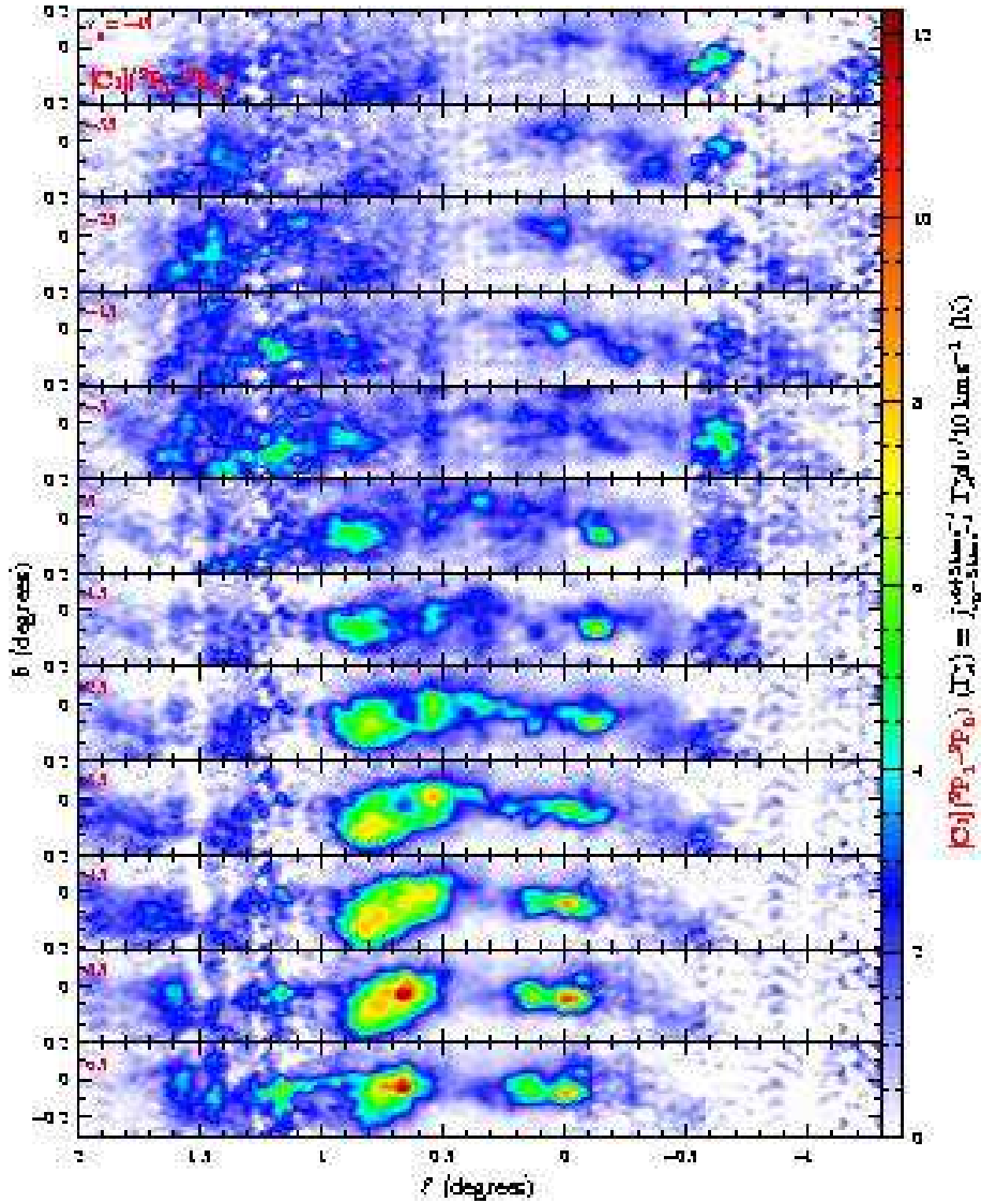


Fig. 4.— *Continued*

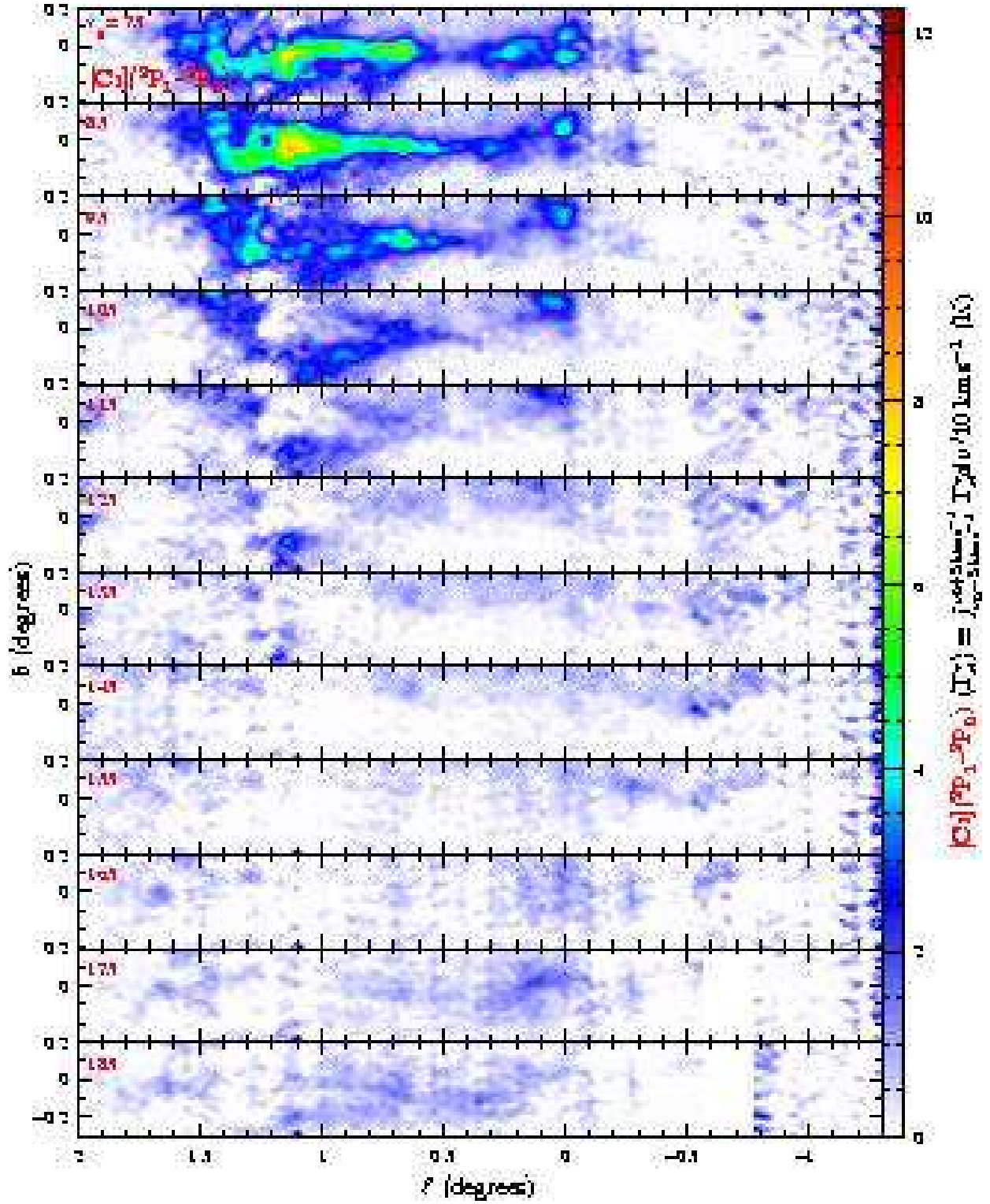


Fig. 4.— *Continued*

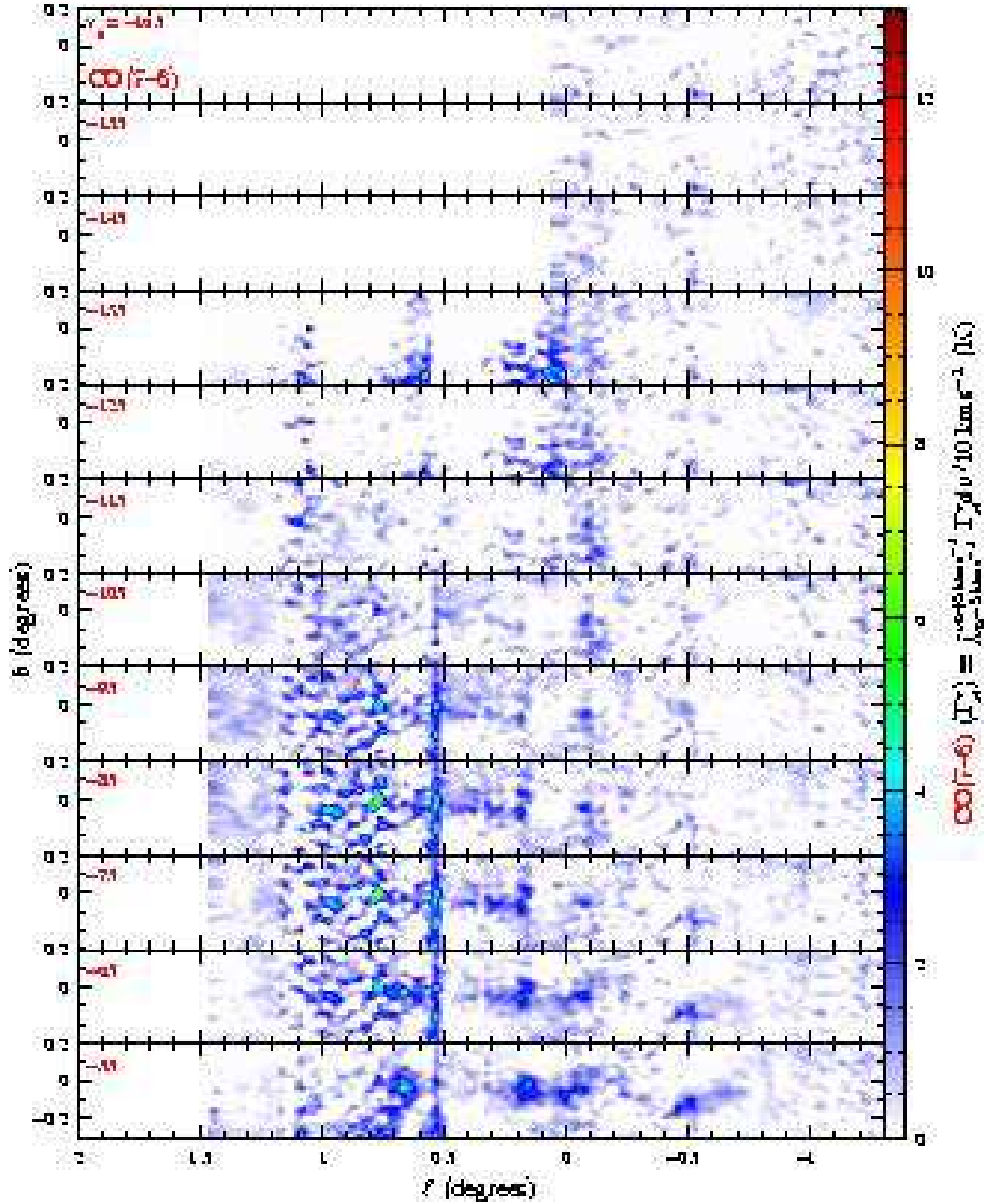


Fig. 5.— False color velocity-channel maps for the CO $J = 7 \rightarrow 6$ transition toward the Galactic Center. Each subpanel shows a 10 km s^{-1} velocity bin, centered at the velocity shown in the upper lefthand corner. The integrated emission in K km s^{-1} has been divided by the 10 km s^{-1} width of the bin so that the color scale at right indicates $\langle T_A^* \rangle$. This figure has been corrected as noted in the erratum.

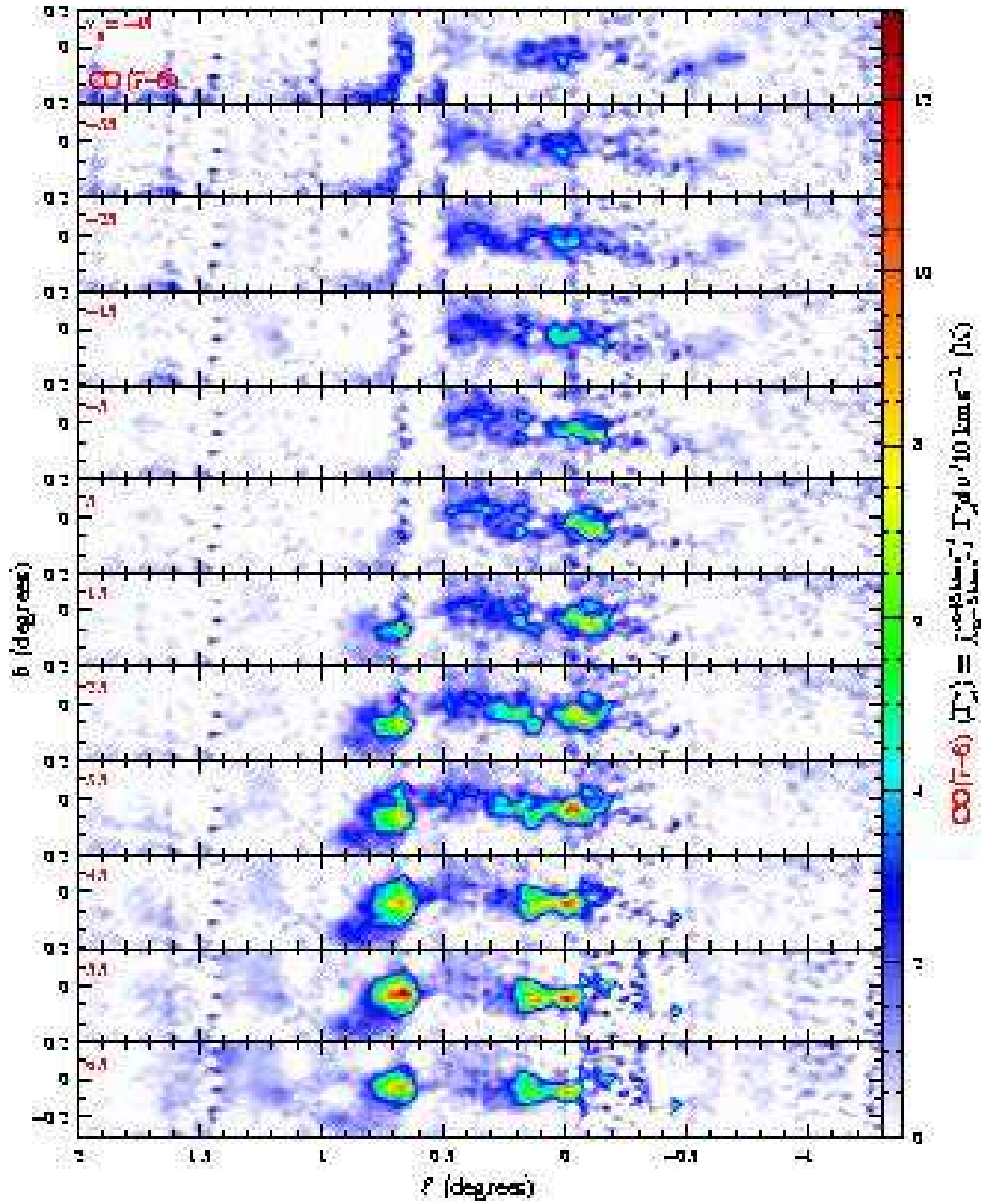


Fig. 5.— *Continued*

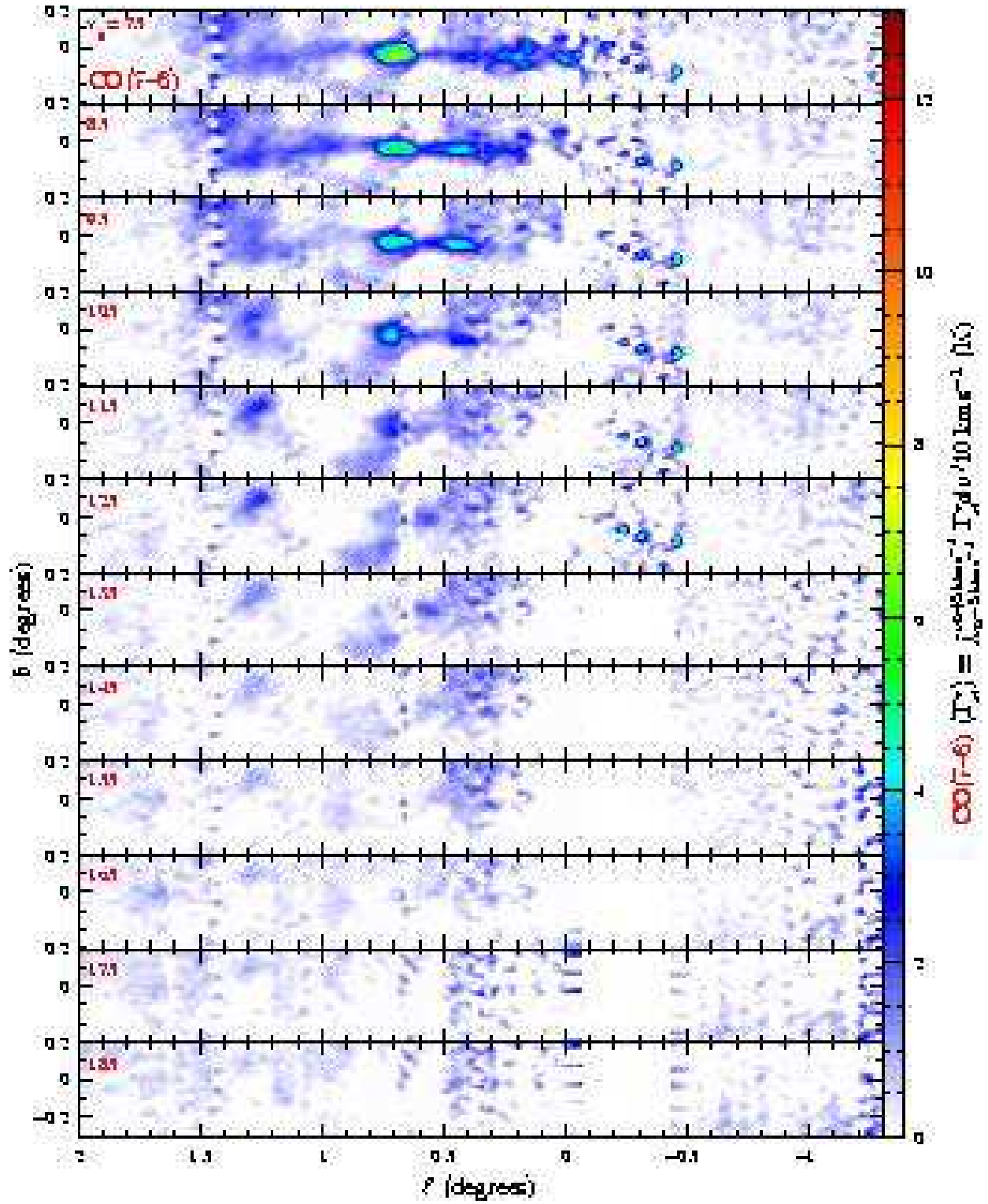


Fig. 5.— *Continued*

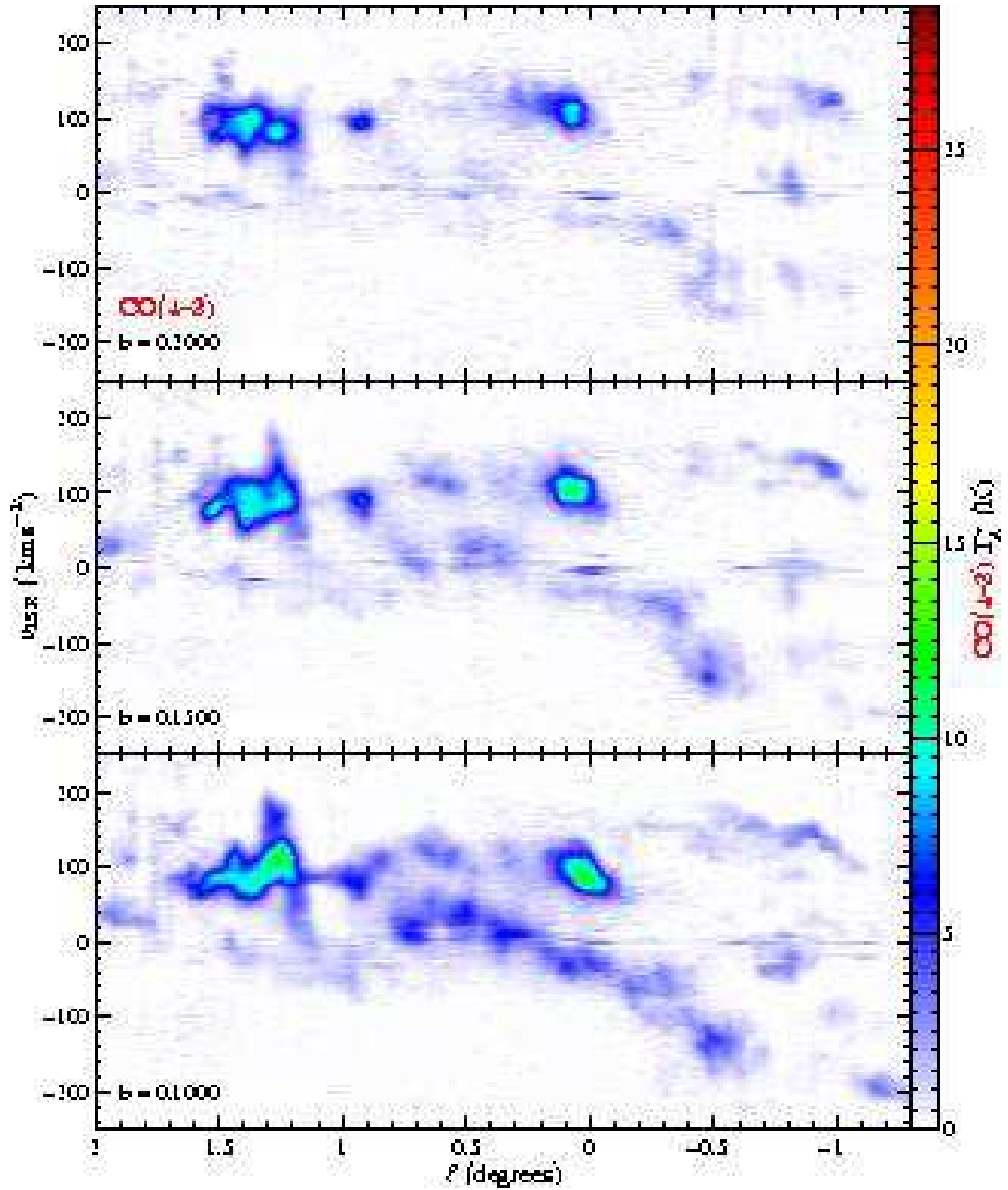


Fig. 6.— False color longitude–velocity maps of CO $J = 4 \rightarrow 3$ emission toward the Galactic Center. Each of the 12 panels displays emission at a different value of galactic latitude, indicated in the lower left corner of each panel.

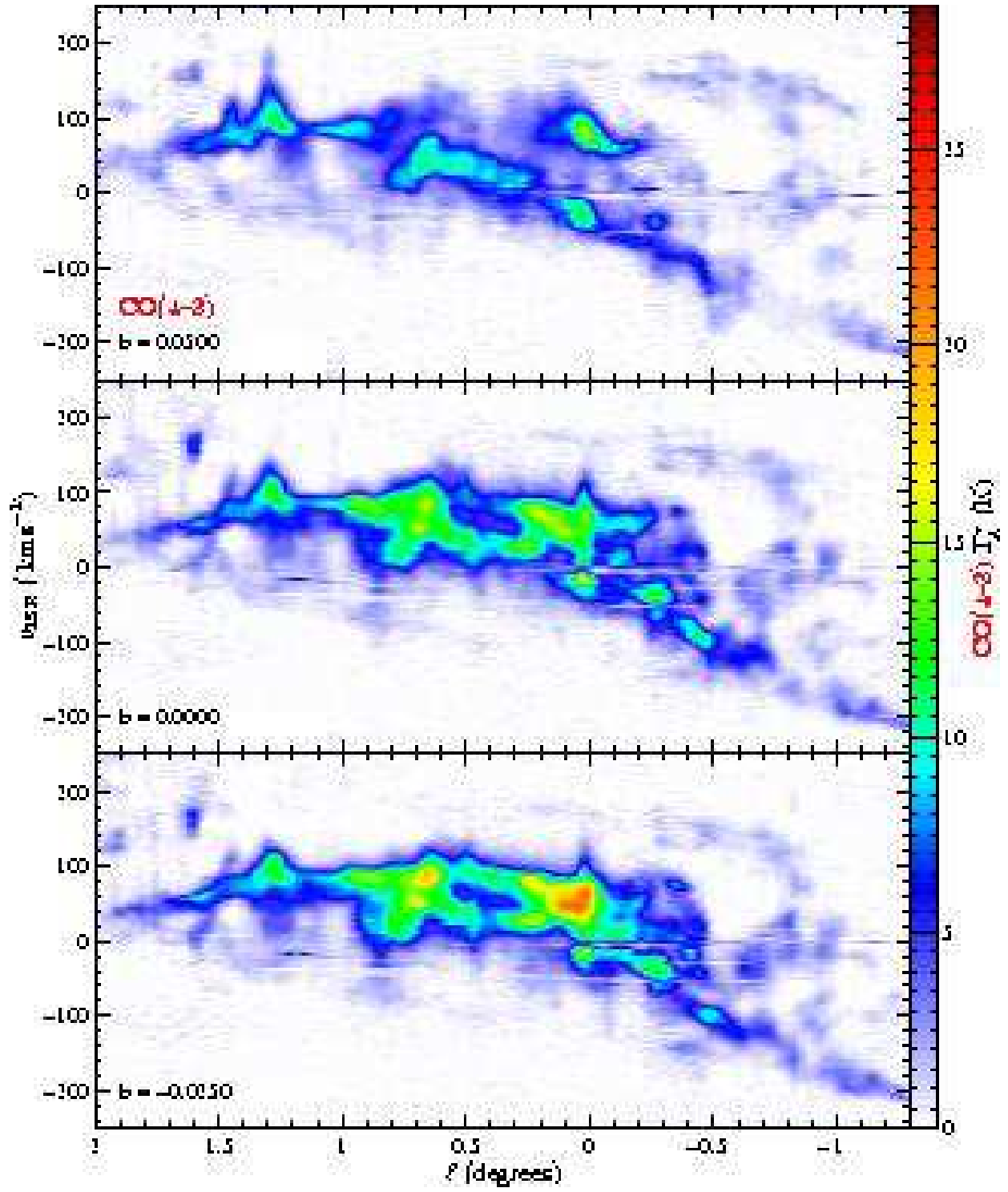


Fig. 6.— *Continued*

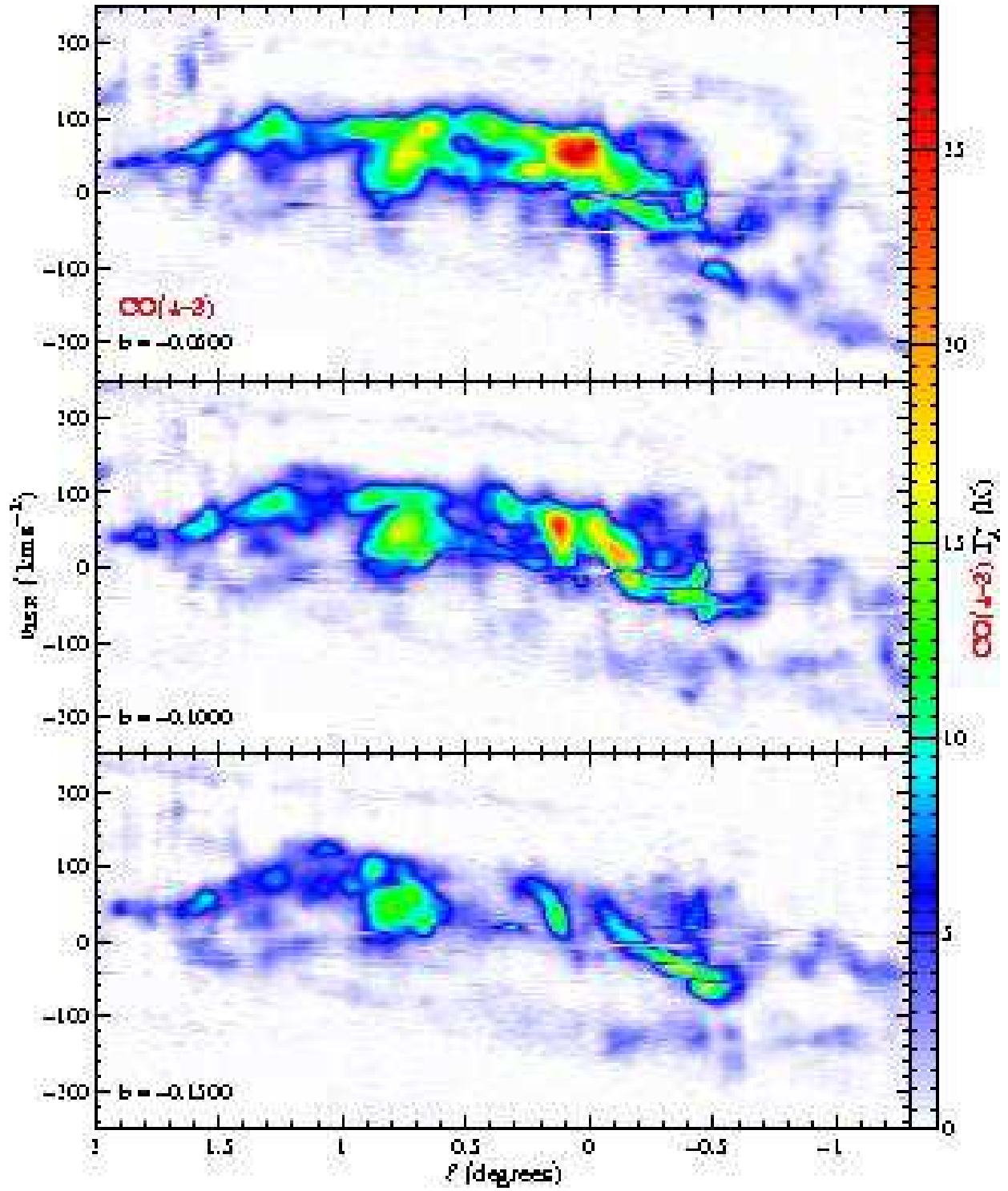


Fig. 6.— *Continued*

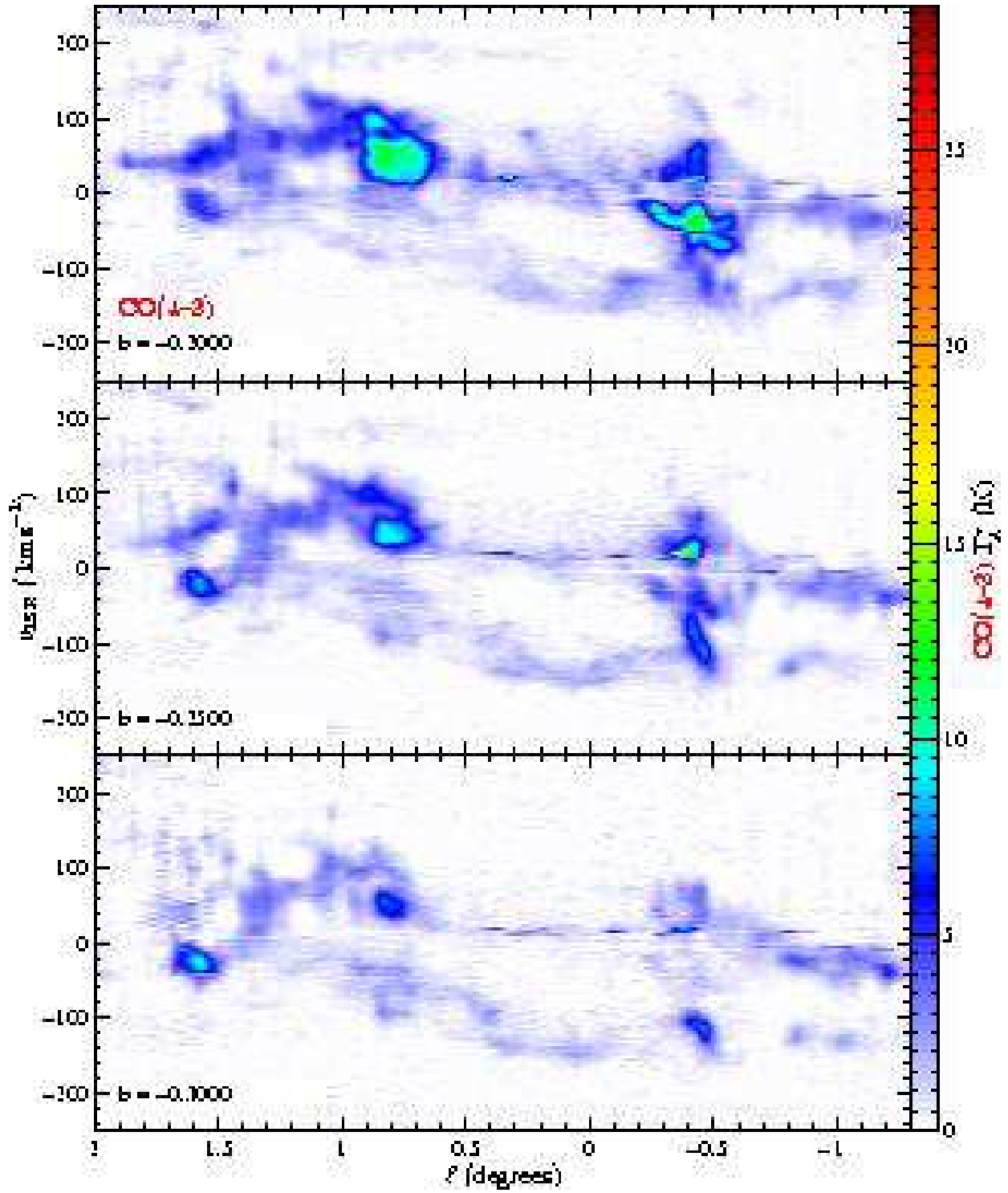


Fig. 6.— *Continued*

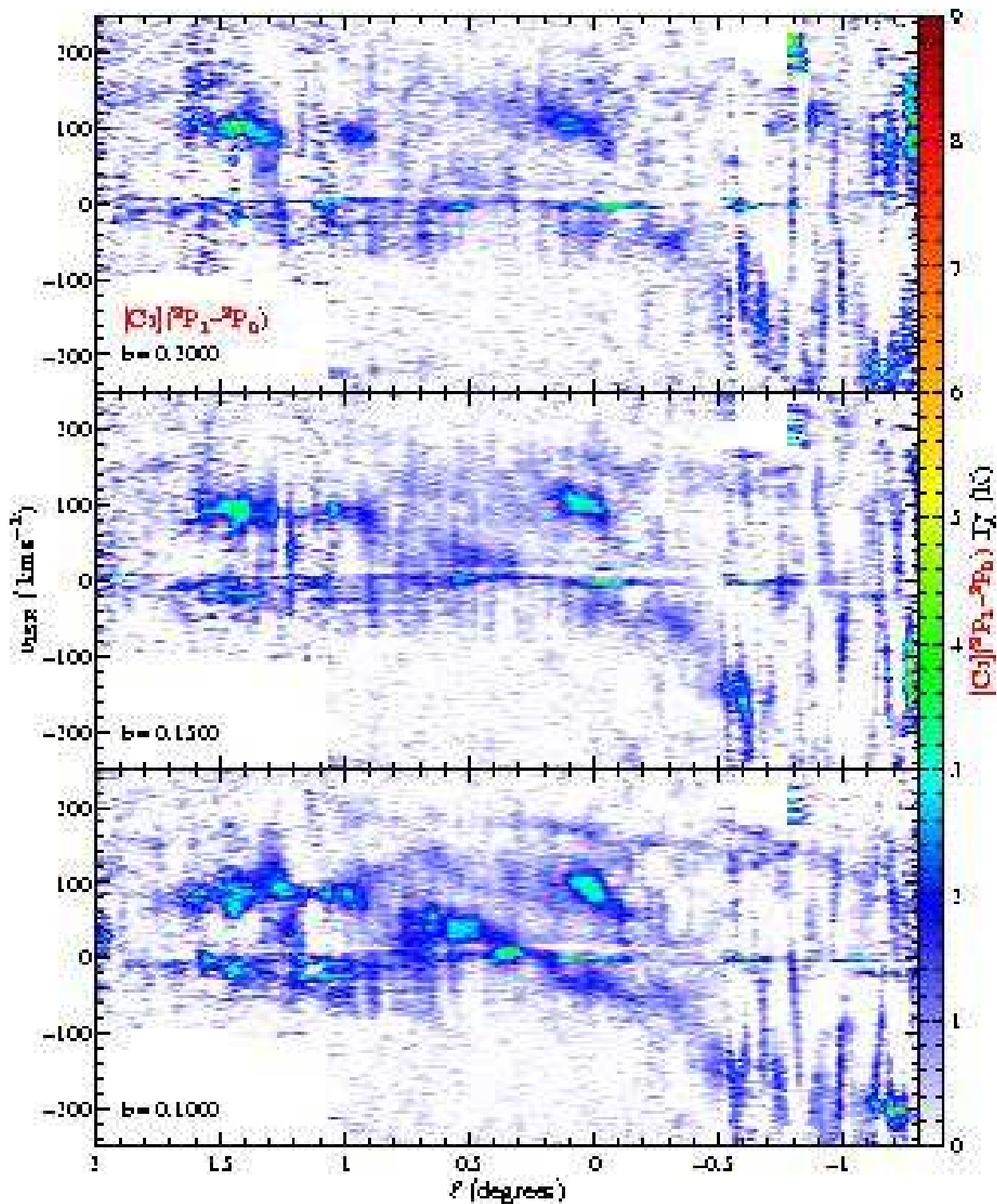


Fig. 7.— False color longitude–velocity maps of $[\text{C I}] \ ^3\text{P}_1 \rightarrow \ ^3\text{P}_0$ emission toward the Galactic Center. Each of the 12 panels displays emission at a different value of galactic latitude, indicated in the lower left corner of each panel.

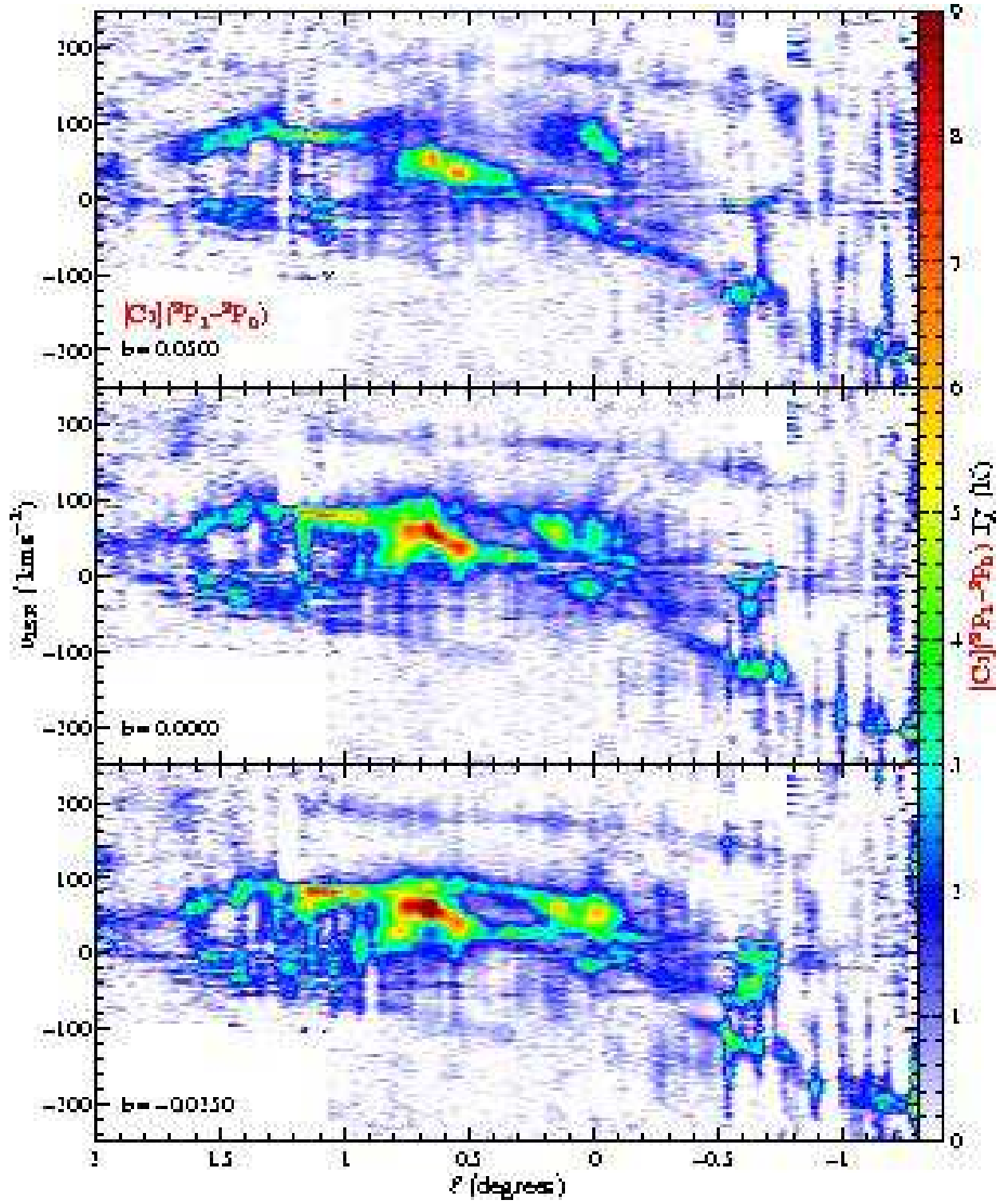


Fig. 7.— *Continued*

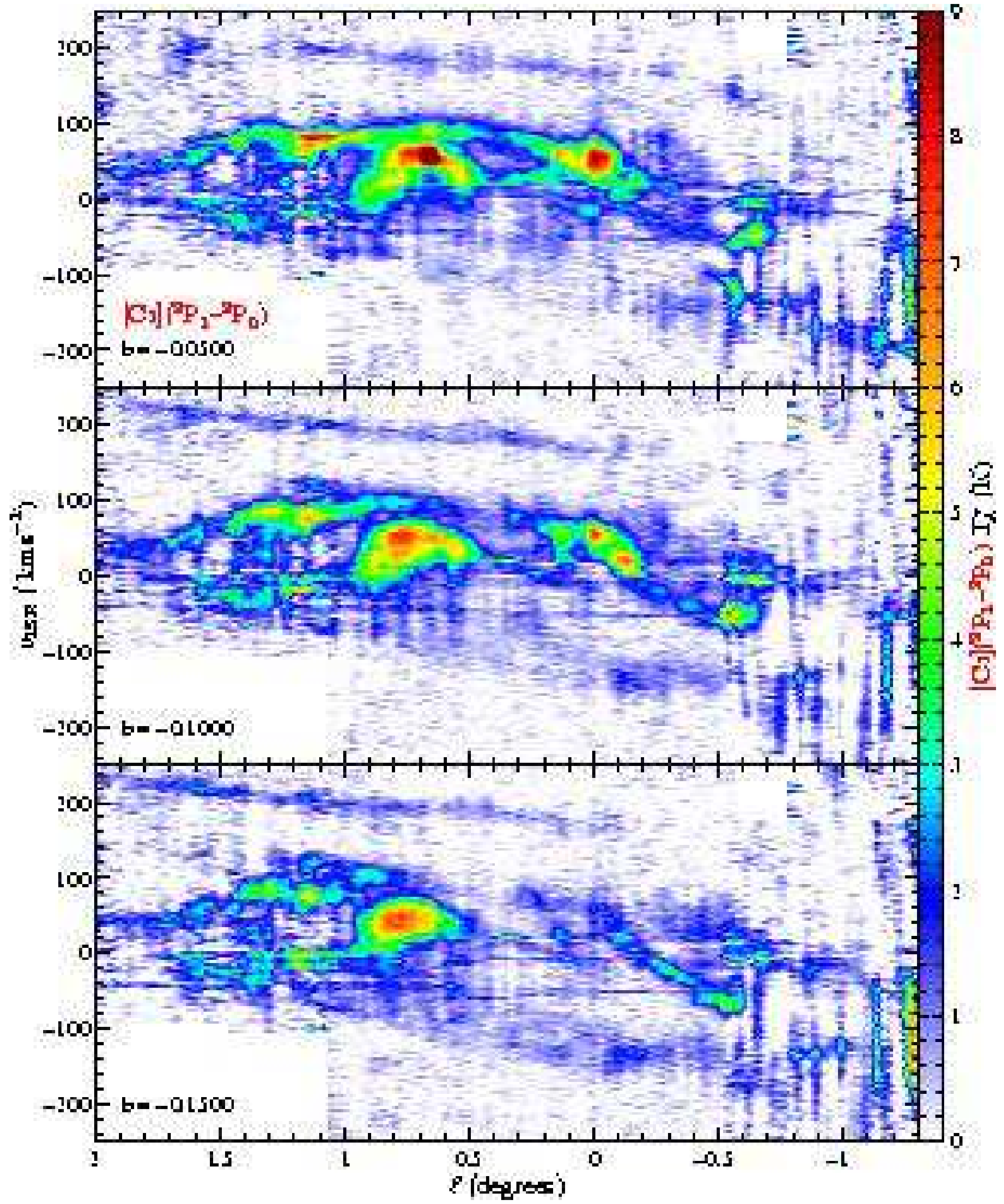


Fig. 7.— *Continued*

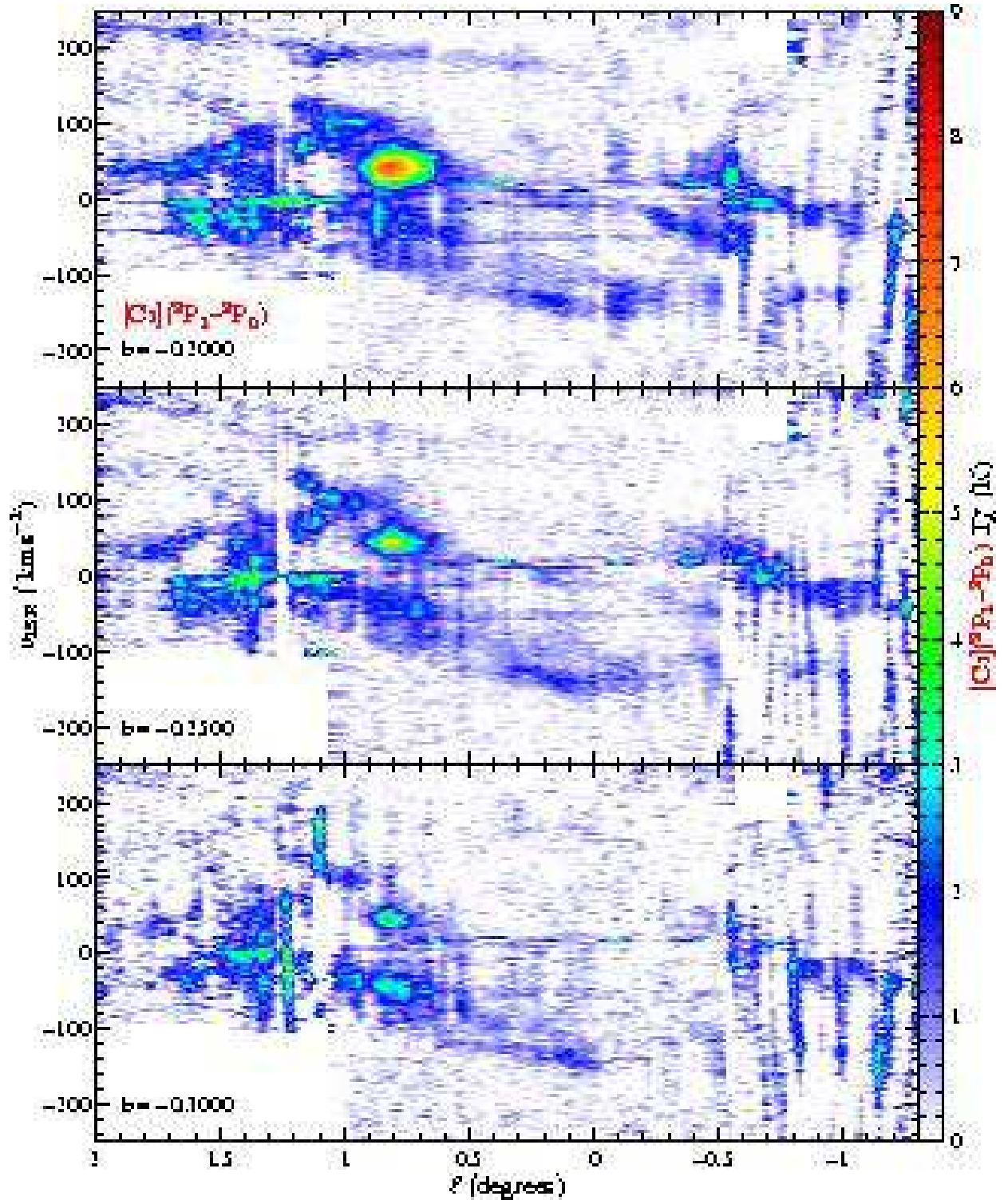


Fig. 7.— *Continued*

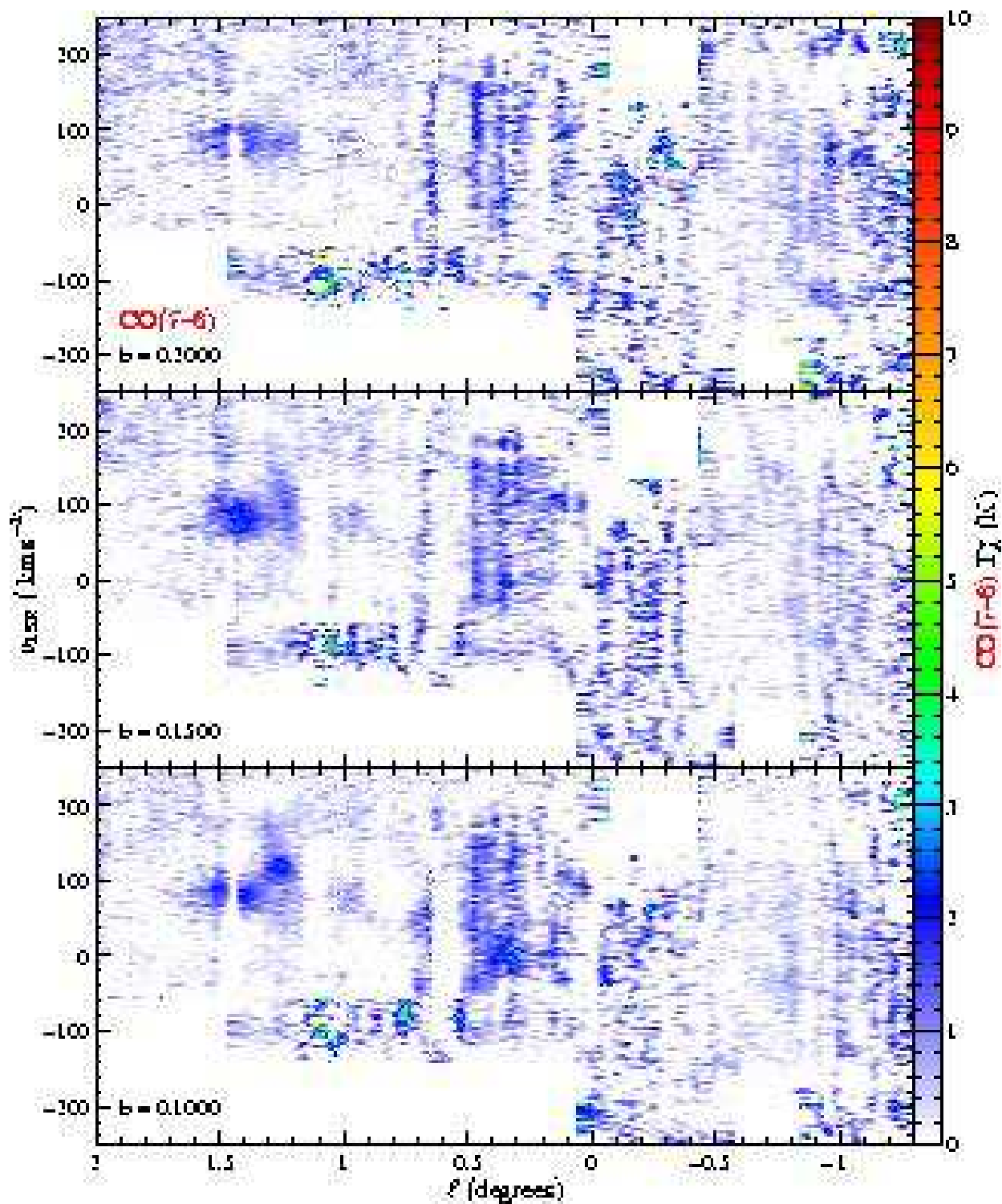


Fig. 8.— False color longitude–velocity maps of CO $J = 7 \rightarrow 6$ emission toward the Galactic Center. Each of the 12 panels displays emission at a different value of galactic latitude, indicated in the lower left corner of each panel.

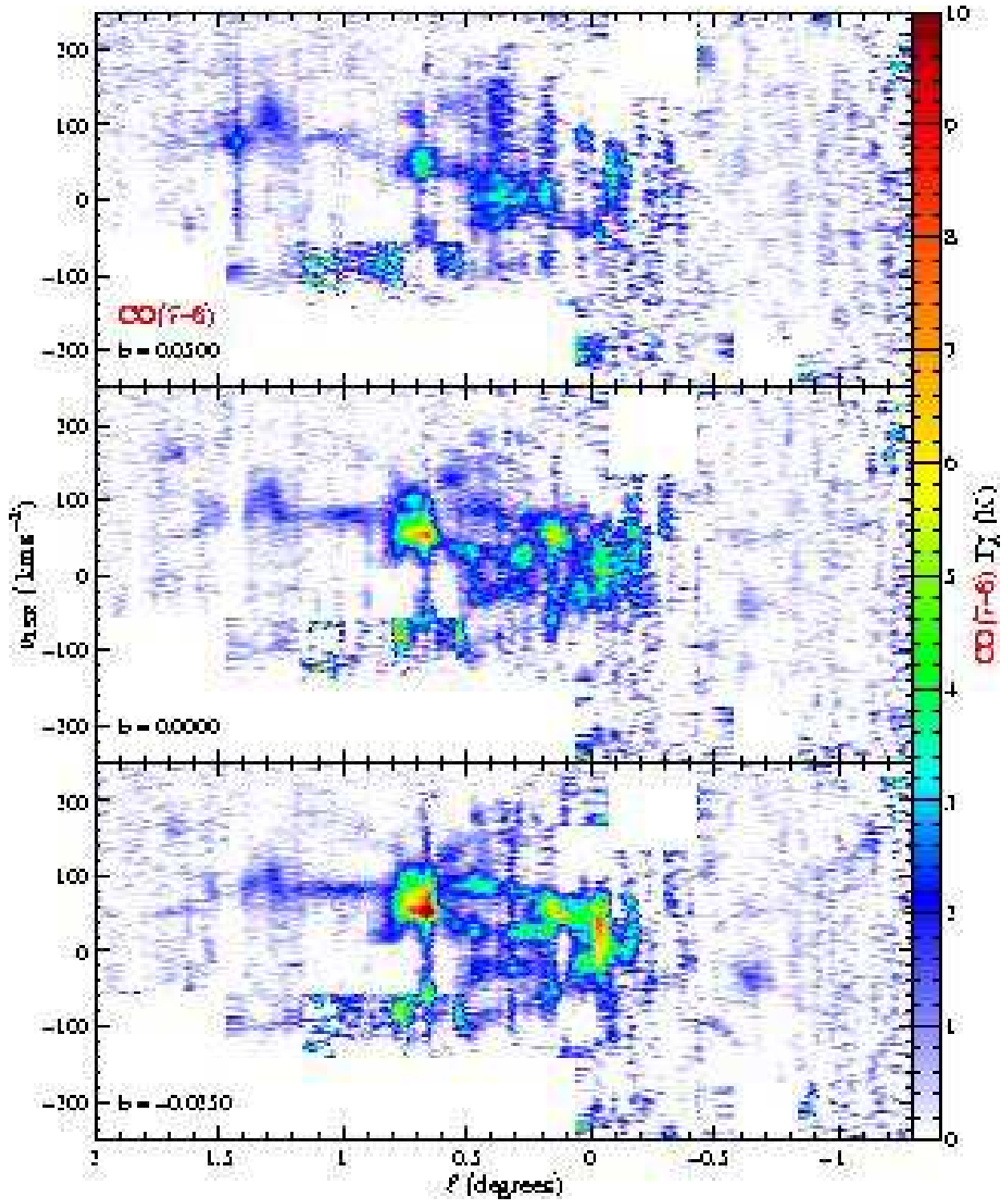


Fig. 8.— *Continued*

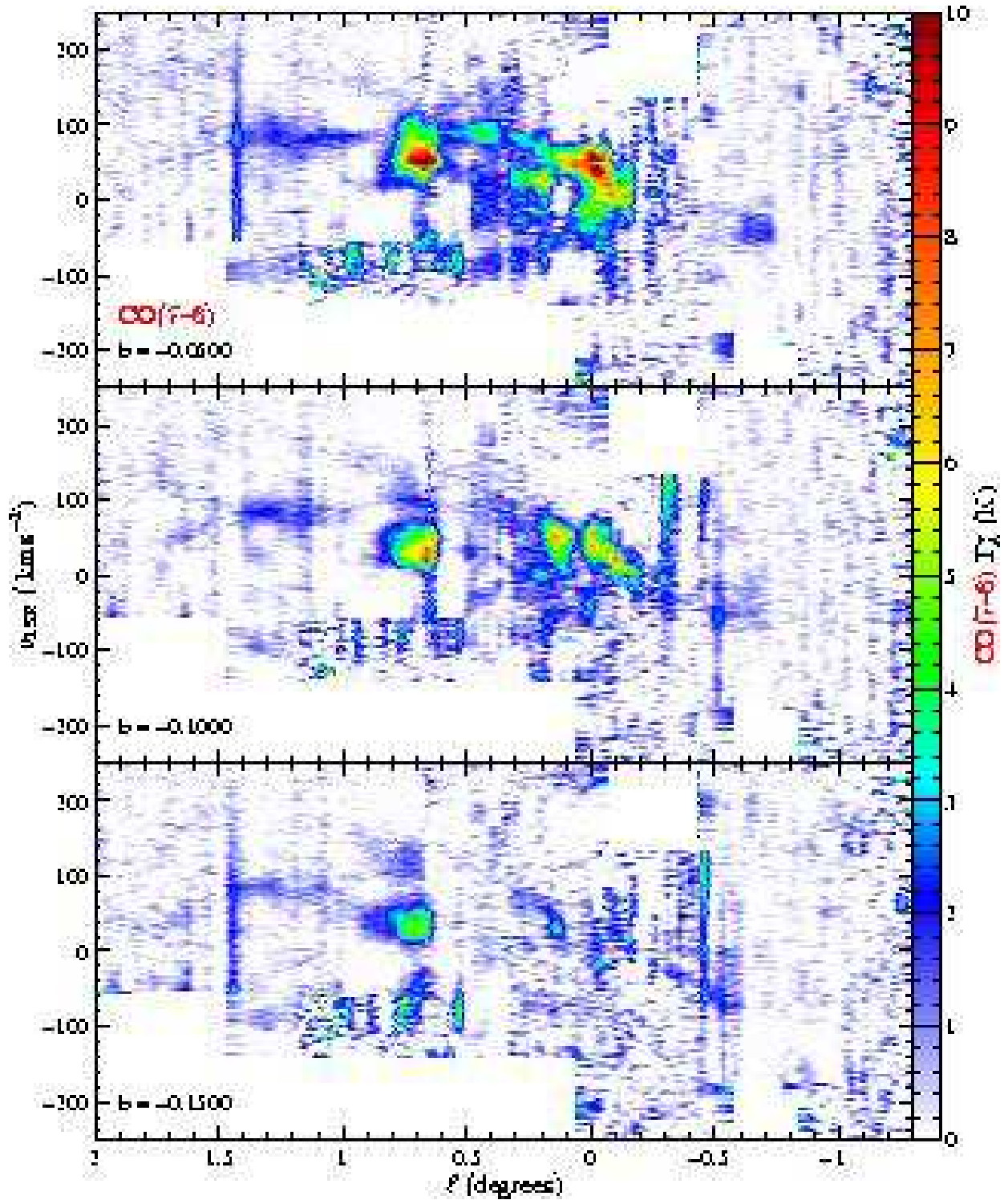


Fig. 8.— *Continued*

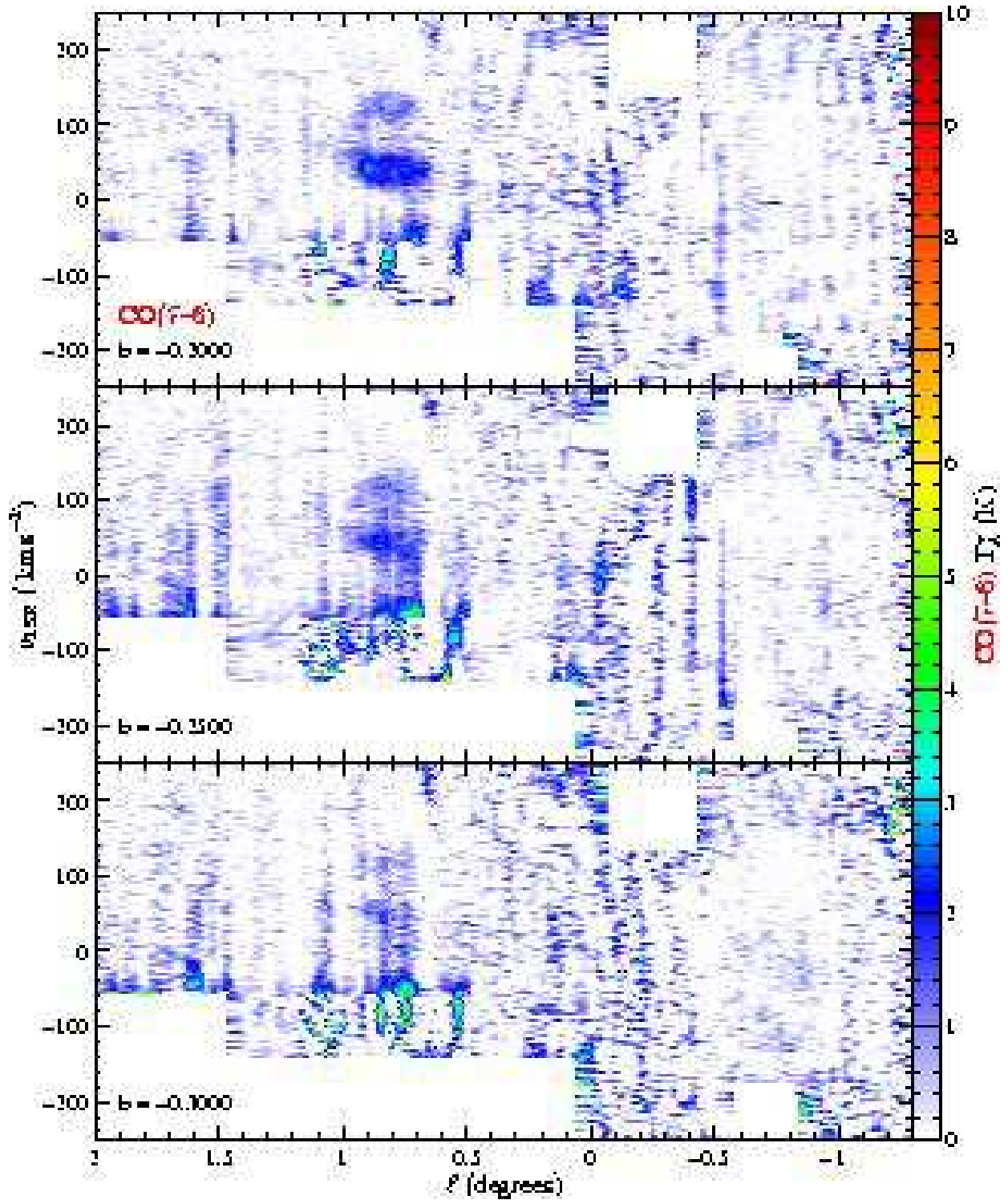


Fig. 8.— *Continued*

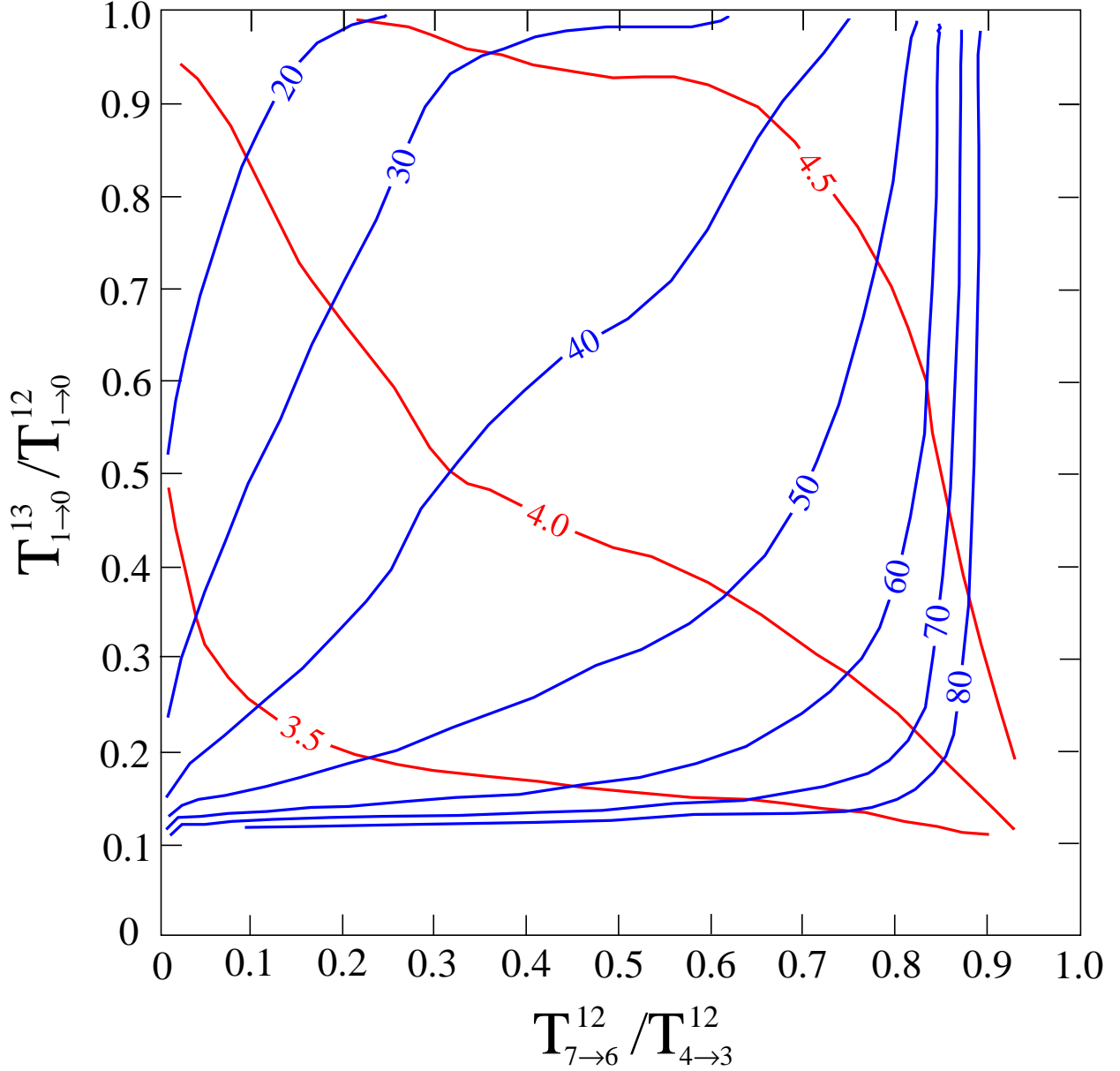


Fig. 9.— Approximate representation of the relation between the line ratios and T_{kin} (blue curves, units are K) and $n(\text{H}_2)$ (red curves, units are $\log[n(\text{H}_2)/1.0 \text{ cm}^{-3}]$) generated by our LVG model, which uses an abundance ratio $^{12}\text{CO}/^{13}\text{CO} = 24$ and $X(\text{CO})/\nabla V = 10^{-4.5} \text{ pc km}^{-1} \text{ s}$. Instabilities in the generation of these functional relationships have been smoothed by hand.

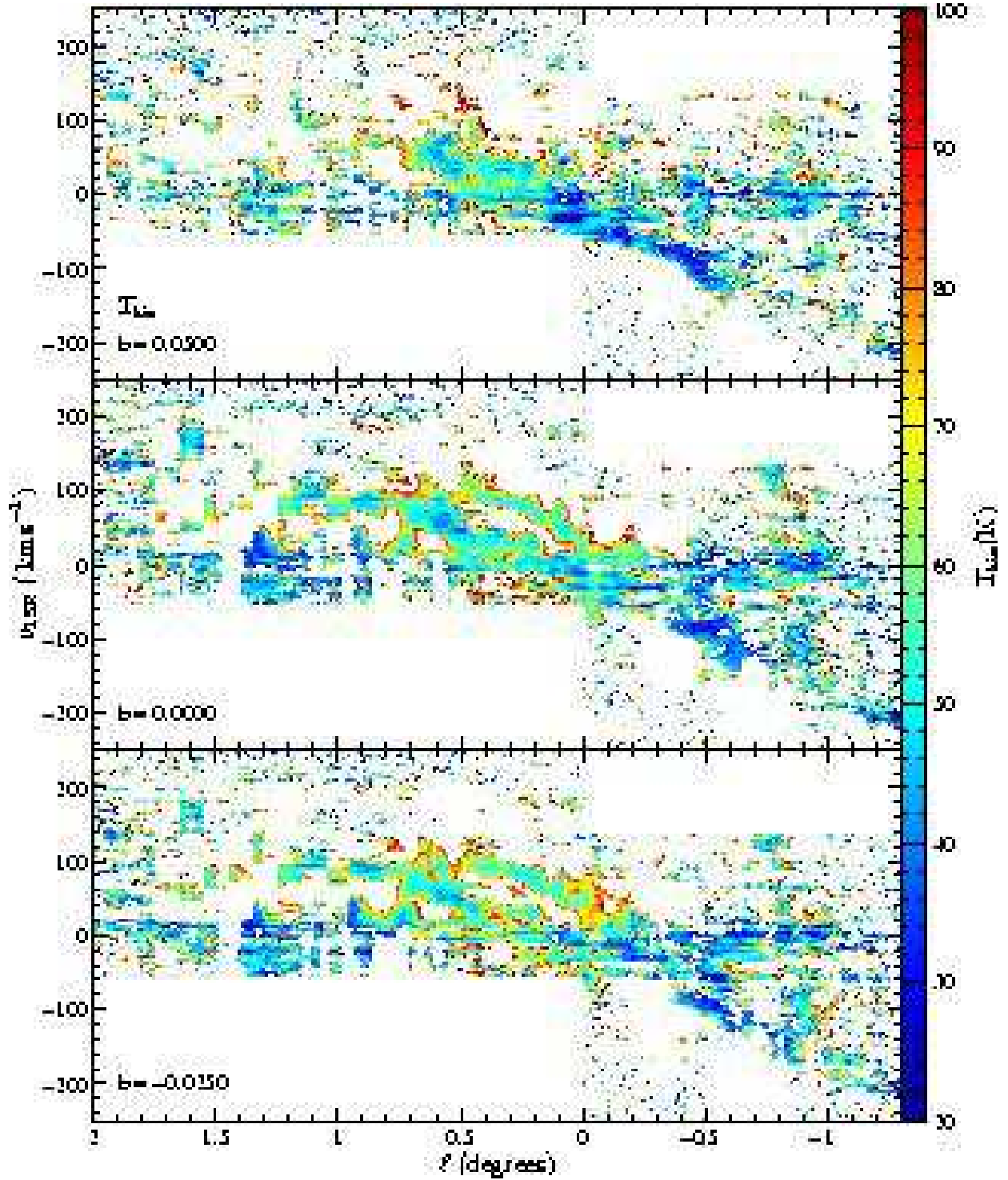


Fig. 10.— False color longitude–velocity maps of T_{kin} as determined by the LVG model described in the text. Regions in white indicate areas where either spectral line data are not available or the LVG model did not converge. Each of the 6 panels displays T_{kin} at a different value of galactic latitude, indicated in the lower left corner of each panel.

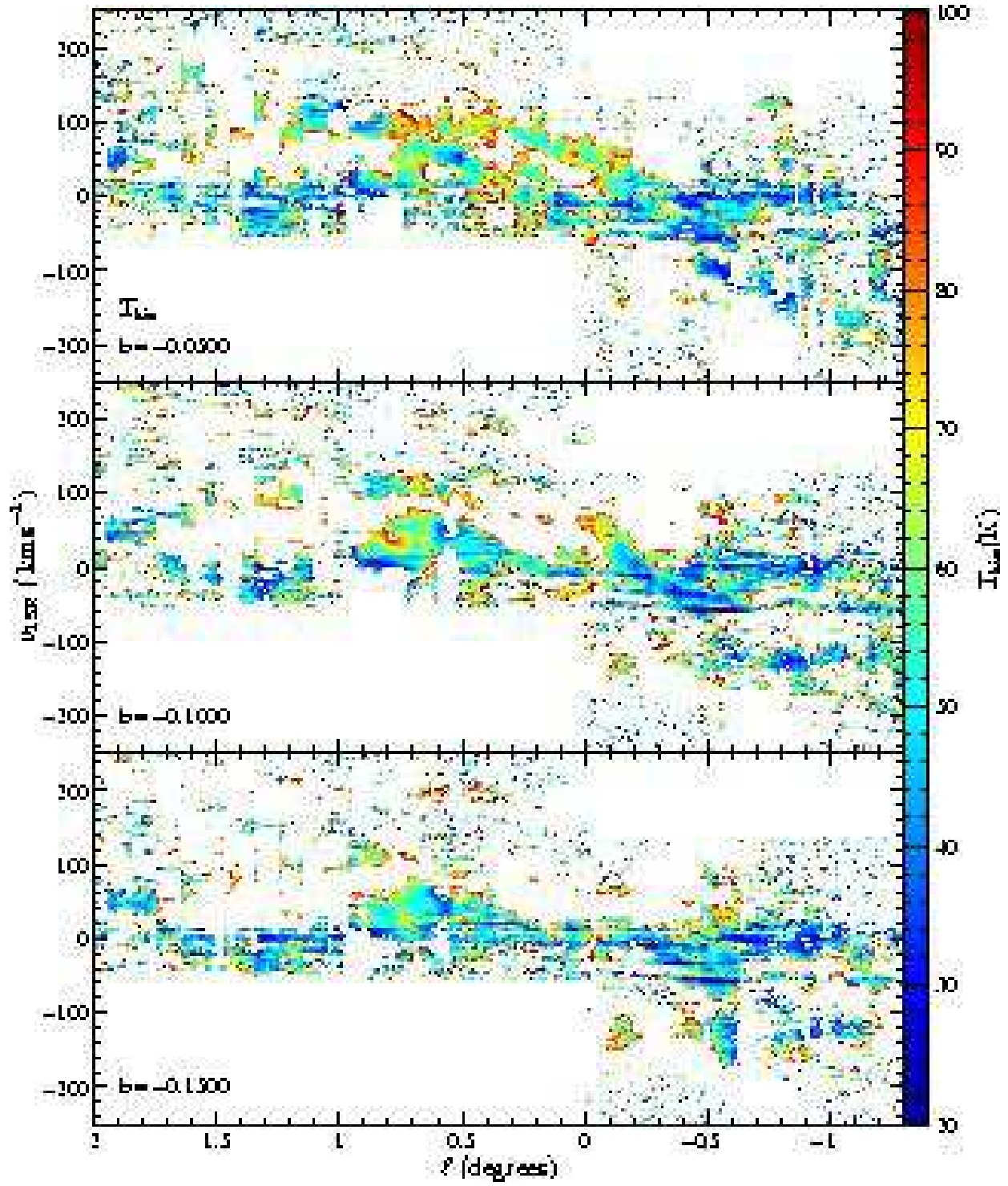


Fig. 10.— *Continued*

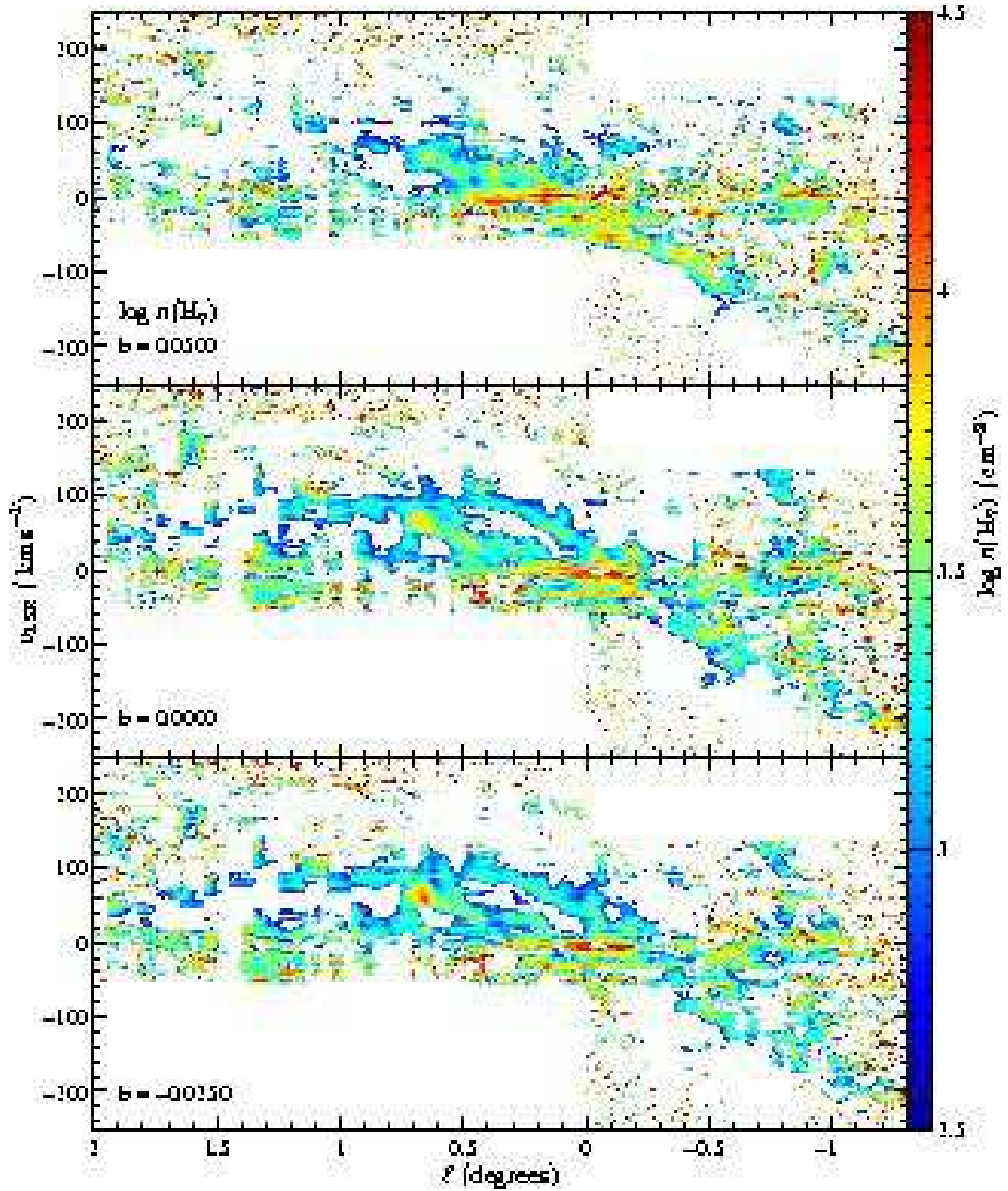


Fig. 11.— False color longitude–velocity maps of $\log n(\text{H}_2)$ as determined by the LVG model described in the text. Regions in white indicate areas where either spectral line data are not available or the LVG model did not converge. Each of the 6 panels displays $n(\text{H}_2)$ at a different value of galactic latitude, indicated in the lower left corner of each panel.

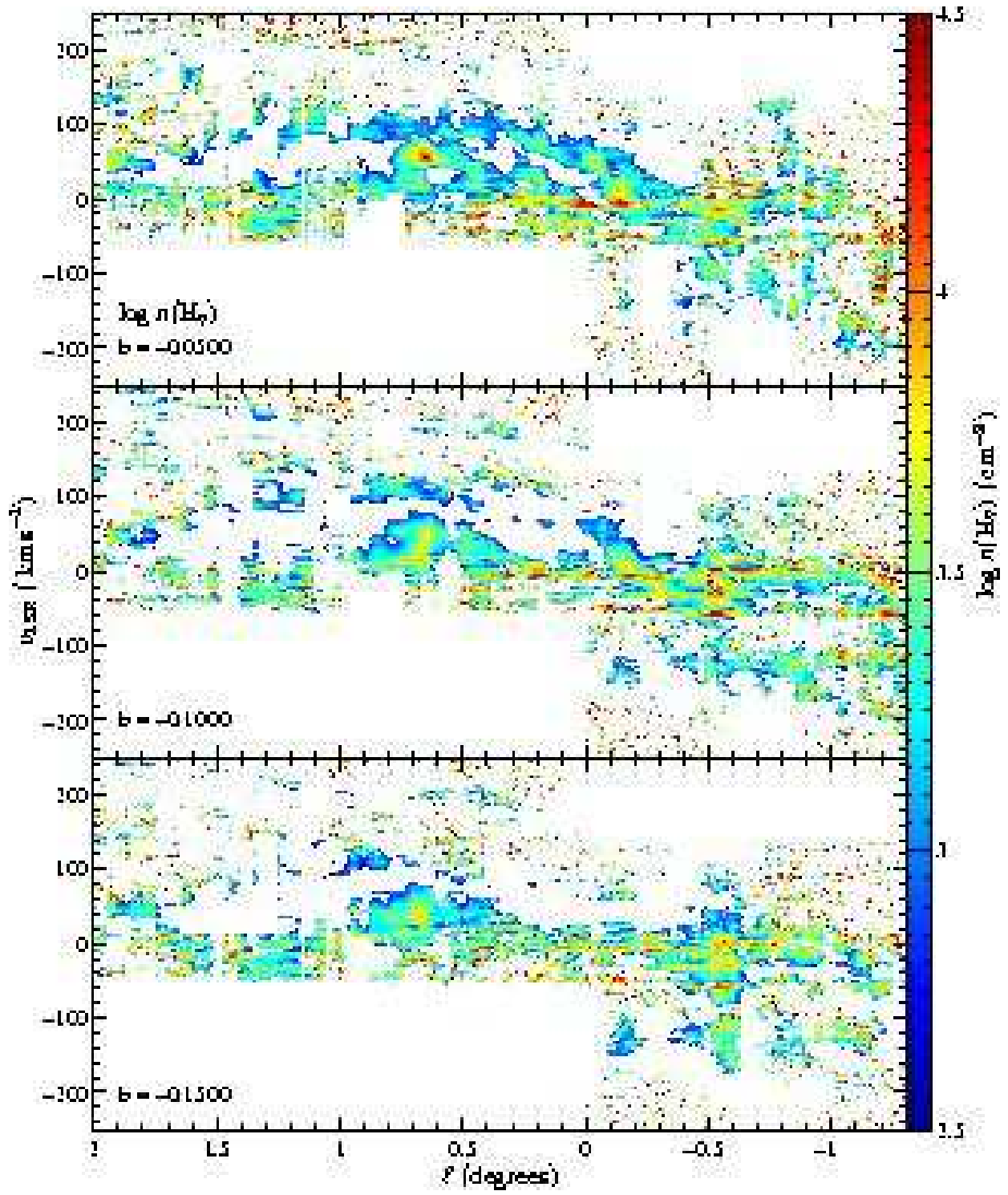


Fig. 11.— *Continued*

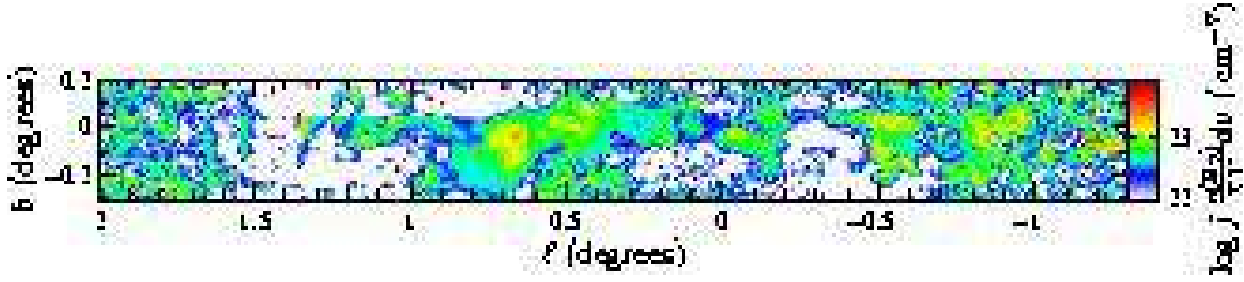


Fig. 12.— False color velocity-channel map of $\log[\int n(\text{H}_2)dv/\nabla V]$ as determined by the LVG model described in the text. $n(\text{H}_2)$ is integrated over the ranges $-150 < v_{\text{LSR}} < -60 \text{ km s}^{-1}$ and $20 < v_{\text{LSR}} < 150 \text{ km s}^{-1}$ in order to avoid contamination by the foreground material for which the LVG analysis is invalid. This value is then divided by ∇V in order to make a map comparable to the expected column density in units of cm^{-2} .